

First-Matsubara-frequency rule in a Fermi liquid.

Part II: Optical conductivity and comparison to experiment

Dmitrii L. Maslov¹ and Andrey V. Chubukov²

¹ *Department of Physics, University of Florida, P.O. Box 118440, Gainesville, FL 32611-8440*

² *Department of Physics, University of Wisconsin-Madison, 1150 Univ. Ave., Madison, WI 53706-1390*

Motivated by recent optical measurements on a number of strongly correlated electron systems, we revisit the dependence of the conductivity of a Fermi liquid, $\sigma(\Omega, T)$, on the frequency Ω and temperature T . Using the Kubo formalism and taking full account of vertex corrections, we show that the Fermi liquid form $\text{Re}\sigma^{-1}(\Omega, T) \propto \Omega^2 + 4\pi^2 T^2$ holds under very general conditions, namely in any dimensionality above one, for a Fermi surface of an arbitrary shape (but away from nesting and van Hove singularities), and to any order in the electron-electron interaction. We also show that the scaling form of $\text{Re}\sigma^{-1}(\Omega, T)$ is determined by the analytic properties of the conductivity along the Matsubara axis. If a system contains not only itinerant electrons but also localized degrees of freedom which scatter electrons elastically, e.g., magnetic moments or resonant levels, the scaling form changes to $\text{Re}\sigma^{-1}(\Omega, T) \propto \Omega^2 + b\pi^2 T^2$, with $1 \leq b < \infty$. For purely elastic scattering, $b = 1$. Our analysis implies that the value of $b \approx 1$, reported for URu₂Si₂ and some rare-earth based doped Mott insulators, indicates that the optical conductivity in these materials is controlled by an elastic scattering mechanism, whereas the values of $b \approx 2.3$ and $b \approx 5.6$, reported for underdoped cuprates and organics, correspondingly, imply that both elastic and inelastic mechanisms contribute to the optical conductivity.

PACS numbers: 71.10.Ay, 71.10. Pm

I. INTRODUCTION

Optical response of strongly correlated materials is an invaluable tool for studying the dynamics of charge carriers.¹ On par with the angular-resolved photoemission spectroscopy which gives information about the single-particle self-energy, optical experiments provide information about two other important quantities: the dynamical effective mass and the scattering rate of conduction electrons.

In the preceding paper² (hereafter referred to as I), we discussed constraints imposed on the functional form of the retarded single-particle self-energy $\Sigma^R(\omega, T)$ by the “first-Matsubara-frequency rule”. This rule stipulates that, under certain conditions, a function obtained by analytic continuation of $\text{Im}\Sigma^R(\omega, T)$ to the Matsubara axis must vanish at the first fermionic Matsubara frequency $\omega \rightarrow \pm i\pi T$. The familiar scaling form of $\text{Im}\Sigma^R(\omega, T)$ in a generic Fermi liquid (FL) in $D > 2$

$$\text{Im}\Sigma^R(\omega, T) = C (\omega^2 + \pi^2 T^2), \quad (1.1)$$

(with a coefficient of exactly π^2 in front of the T^2 term), obviously satisfies this rule.

In the present paper, we discuss a similar constraint—“the first bosonic Matsubara-frequency rule”—imposed on the scaling form of the optical conductivity $\sigma(\Omega, T)$.

Within the semiclassical Boltzmann equation, the T^2 -scaling of the dc resistivity due to Umklapp electron-electron scattering was obtained by Landau and Pomeranchuk,³ and due normal scattering in a two-band metal by Baber.⁴ Later on, Eliashberg⁵ re-derived this result from the Kubo formula, and showed that it remains valid to all orders in the electron-electron interaction. The Ω/T scaling of the “optical resistivity” of a 3D

FL was first discussed by Gurzhi,⁶ who used a quantum Boltzmann equation to show that

$$\text{Re}[\rho(\Omega, T)] \equiv \text{Re}[\sigma^{-1}(\Omega, T)] = A' [\Omega^2 + 4\pi^2 T^2]. \quad (1.2)$$

The Ω and T dependences of $\text{Re}\rho(\Omega, T)$ are similar to those of the leading term in $\text{Im}\Sigma^R(\omega, T)$ [cf. Eq. (1.1)], but the ratio of the T^2 and Ω^2 terms is now $4\pi^2$ instead of π^2 .

This difference is not accidental. Indeed, $\text{Im}\Sigma^R(\omega, T)$ measures the decay rate of single-particle excitations, which are fermions; hence the thermal part of $\text{Im}\Sigma^R(\omega, T)$ contains the square of first fermionic Matsubara frequency ($= \pi T$) rather than T itself. On the other hand, $\text{Re}\rho(\Omega, T)$ measures the decay rate of current fluctuations, which are bosons; hence the thermal part of $\text{Re}\rho(\Omega, T)$ contains the square of the first (non-zero) bosonic Matsubara frequency ($= 2\pi T$). Also not coincidentally, Eq. (1.2) is of the same form as the sound absorption rate in FLs.⁷

To the best of our knowledge, the scaling form predicted by Eq. (1.2) has never been verified experimentally in conventional metals. On the other hand, the Ω/T scaling of $\text{Re}\rho(\Omega, T)$ has been studied intensively in strongly correlated materials, e.g., in heavy-fermion metals and doped Mott insulators. The result of these studies is quite surprising: whenever it was possible to fit the Ω and T dependencies of $\text{Re}\rho(\Omega, T)$ by quadratic functions, the coefficient $b \equiv \pi^2 T^2 / \Omega^2$ was found to be quite different from 4. This issue was highlighted by recent study⁸ of $\text{Re}\rho(\Omega, T)$ in the “hidden-order” (HO) heavy-fermion compound URu₂Si₂, where b was found to be close to 1 above the 17.5 K transition to the HO state. In fact, the value of $b \approx 1$ was found in a number of other materials, including two rare-earth based doped Mott insulators,

$\text{Nd}_{0.905}\text{TiO}_3$ (Ref. 9) and $\text{Ce}_{0.095}\text{Ca}_{0.05}\text{TiO}_{3.04}$ (Ref. 10). Another recent study¹¹ reports $b \approx 2.3$ in the underdoped cuprate $\text{HgBa}_2\text{CuO}_{4+\delta}$. Whereas the observed value of b is less than 4 in most of the cases, there is one exception: $b \approx 5.6$ was reported for a quasi-two-dimensional (2D) organic material of the BEDT-TTF family.¹² A deviation of b from 4 can also be inferred from the optical data on UPt_3 ,¹³ Sr_2RuO_4 ,¹⁴ and Cr ;¹⁵ see Ref. 8 for more details.

Motivated by these findings, we revisit the Ω/T scaling of the optical conductivity of a FL in this paper. We extend the Eliashberg's analysis of the Kubo formula for the conductivity to finite Ω and obtain an expression for $\sigma(\Omega, T)$ to all orders in the electron-electron interaction. To discuss the results, it is convenient to identify two distinct frequency regimes, the "high-frequency" and "low-frequency" ones, and also two types of FLs, the "conventional" and "non-conventional" ones.

As far as the frequency regimes are concerned, Ω is larger than $\text{Im}\Sigma^R(\Omega, T)$ in the high-frequency regime, while $\Omega < \text{Im}\Sigma^R(\Omega, T)$ in the low-frequency one. (The low-frequency regime also includes the dc limit of $\Omega = 0$.) In the context of the standard Drude formula, these regimes are also referred to as "non-dissipative" or "reactive" and "dissipative", correspondingly.

Turning to two types of FLs, we define a "conventional FL" as such in which the leading ω and T dependencies of $\text{Im}\Sigma^R(\omega, T)$ are given by $\omega^2 + \pi^2 T^2$, as in Eq. (1.1), while the higher-order terms may be non-analytic. In a "nonconventional FL", already the leading term in $\text{Im}\Sigma^R(\omega, T)$ is a non-analytic function of ω and T . For a wide class of interactions that remain finite at $q = 0$, the demarcation line between the two types of FLs is determined by the dimensionality: the case of $D > 2$ corresponds to conventional FLs, while the case of $1 < D < 2$ corresponds to non-conventional FLs. In the latter case, $\text{Im}\Sigma^R(\omega, 0) \propto |\omega|^D$ and $\text{Im}\Sigma^R(0, T) \propto T^D$. In the marginal case of $D = 2$, $\text{Im}\Sigma^R(\omega, 0) \propto \omega^2 \ln|\omega|$ and $\text{Im}\Sigma^R(0, T) \propto T^2 \ln T$.

In the high-frequency regime, current-carrying quasiparticles can be considered as nearly free, so that the residual interaction among quasiparticles, which gives rise to their finite lifetime, can be treated as a perturbation. We show that in this regime $\text{Re}\rho(\Omega, T)$ is given by Eq. (1.2) for both conventional and non-conventional FLs, as well as for the marginal case of $D = 2$, despite qualitative differences in the self-energies in these cases. Our analysis keeps full track of the vertex corrections to the conductivity and thus takes both normal and Umklapp scattering processes into account. We argue that the $4\pi^2$ coefficient of the T^2 term in this formula is a consequence of the "bosonic first-Matsubara-frequency rule", which stipulates that a function obtained by analytic continuation of $\text{Re}\rho(\Omega, T)$ to the first (non-zero) bosonic Matsubara frequency, $\Omega \rightarrow \pm 2i\pi T$, does not have a T^2 term. Equation (1.2) obviously obeys this rule.

In the low-frequency regime, $\text{Re}\rho(\Omega, T)$ differs from Eq. (1.2) because the interaction among quasiparticles

can no longer be treated as a perturbation, and this affects the T^2 and Ω^2 terms in $\text{Re}\rho(\Omega, T)$ in different ways. We analyzed the change in the functional form of $\rho(\Omega, T)$ between the high- and low-frequency regimes in the "zero-bubble approximation"¹⁶ and found that the change is numerically quite small, i.e., the formula

$$\text{Re}\rho(\Omega, T) = A' (\Omega^2 + b\pi^2 T^2) \quad (1.3)$$

with $b \approx 4$ remains quite accurate down to the lowest Ω , although the exact form of $\text{Re}\rho(\Omega, T)$ in the entire range of Ω is different from that in Eq. (1.2). We also analyzed $\text{Re}\rho(\Omega, T)$ in the "incoherent regime", where all energy scales are of the same order, i.e., $\Omega \sim T \sim \text{Re}\Sigma^R(\Omega, T) \sim \text{Im}\Sigma^R(\Omega, T)$, and again found a good fit by the $\Omega^2 + b\pi^2 T^2$ form with $b \approx 4$.

Equation (1.3) is to be taken with some caution, because the zero-bubble approximation neglects the corrections to the current vertex in the polarization bubble. Physically, vertex corrections differentiate between normal and Umklapp scattering processes. In the high-frequency regime, both normal and Umklapp processes contribute to the resistivity provided that the Fermi surface (FS) is sufficiently anisotropic^{6,17,18} (a precise definition of "sufficiently anisotropic" is given in Sec. IV). As a result, Eq. (1.2) remains valid when the vertex corrections are included. The only change is that the prefactor A' now contains a sum of normal and Umklapp scattering amplitudes. In the low-frequency regime and, in particular, at $\Omega = 0$, the resistivity of an impurity-free system is non-zero only in the presence of Umklapp scattering, although normal processes also contribute once Umklapp processes are allowed.¹⁹ As a result, the prefactor A in the dc resistivity

$$\rho(0, T) = 4\pi^2 AT^2 \quad (1.4)$$

contains some function of the normal and Umklapp scattering amplitudes rather than just their sum, and is therefore different from A' in the high-frequency limit. What remains to be seen is how the functional form of $\text{Re}\rho(\Omega, T)$ evolves between the dc and high-frequency limits beyond the zero-bubble approximation.

We then discuss the experiment, focusing mostly on recent optical measurements on URu_2Si_2 .⁸ Given that the observed values of the coefficient b are substantially different from the FL value $b = 4$, we argue that the existing optical data cannot be explained only by the electron-electron interaction. Following an analogy with the Kondo effect,²⁰ we propose a phenomenological model which, in addition to electron-electron scattering, contains also *elastic* scattering by some localized degrees of freedom, e.g., magnetic moments or resonant levels. In this model, the self-energy is a sum of two parts: the elastic one, described by an ω^2 term, and the inelastic one, described by the standard FL term, $\omega^2 + \pi^2 T^2$, i.e.,

$$\text{Im}\Sigma^R(\omega, T) = C [a\omega^2 + (\omega^2 + \pi^2 T^2)], \quad (1.5)$$

where the relative weight of the elastic and inelastic contributions, a , is an adjustable parameter of the model.

Within the zero-bubble approximation, the coefficient b in Eq. (1.3) is related to a via

$$b = \frac{a+4}{a+1}. \quad (1.6)$$

For practical purposes, the model is meaningful only for $-1 < a < \infty$; consequently, $1 \leq b < \infty$. The FL value of $b = 4$ is reproduced for $a = 0$. The opposite limit of $a = \infty$ (and thus $b = 1$) corresponds to a purely elastic scattering mechanism. The range $1 < b < 4$ corresponds to a mixture of elastic and inelastic mechanisms with $a > 0$, whereas $b > 4$ corresponds to an elastic contribution with $-1 < a < 0$.

In this classification scheme, the value of $b \approx 1$, reported in Refs. 8–10, indicates a purely elastic scattering mechanism, whereas $b \approx 2.3$ (and thus $a \approx 1.3$) and $b \approx 5.6$ (and thus $a \approx -0.35$), reported in Refs. 11 and 12, correspondingly, point at a mixture of elastic and inelastic mechanisms with opposite signs of the elastic contribution.

We discuss one possible mechanism that leads to $b \approx 1$, i.e., scattering at resonant levels, and show that this mechanism explains the data on URu₂Si₂ reasonably well. We refrain from identifying the microscopic origin of the resonant levels (except for noting that *extrinsic* resonant impurities can hardly be the culprits) but merely surmise that *intrinsic* deep electron states can play a role of incoherent resonant scatterers at relatively high energies, where a coherent Bloch state is not formed yet.

Whereas the resonant-level model explains the optical data in the “ $b = 1$ ” materials, the T dependence of the dc resistivity can be explained only by invoking a sufficiently strong electron-electron interaction which, when combined the resonant elastic scattering, does not significantly affect the optical scattering rate. We show that dc and optical measurements probe different scattering mechanisms: while a dc measurement is sensitive to both elastic and inelastic mechanisms, an optical measurement probes primarily the elastic channel,

The rest of the paper is organized as follows. In Sec. II we discuss the optical conductivity of a FL in the high-frequency regime within the Kubo formalism. In Sec. III, we extend the analysis to both the low-frequency and incoherent regimes within the zero-bubble approximation for the current-current correlator. In Sec. IV, we discuss the interplay between normal and Umklapp contributions to the resistivity in different frequency regimes. Section V addresses comparison to the experiment. In Sec. V A, we discuss the status of the experiment and conclude that it cannot be explained within the model which includes only the electron-electron interaction. In Sec. V B, we introduce a phenomenological model which combines elastic and inelastic scattering mechanisms, and classify the observed values of the coefficient b within this model. In Sec. V C, we apply the resonant-scattering model to the data on URu₂Si₂. Section VI presents our conclusions.

II. OPTICAL CONDUCTIVITY

OF A FERMI LIQUID

A. Kubo formula: rigorous treatment

1. Preliminaries

As in I, we consider an electron system on a lattice. We assume that the FS does not have nested parts and is away from van Hove singularities but is otherwise arbitrary. Near the FS, the bare electron dispersion, $\varepsilon_{\mathbf{k}}^0$, (measured from the Fermi energy) is approximated by $\varepsilon_{\mathbf{k}}^0 = \mathbf{v}_{\mathbf{k}_F}^0 \cdot (\mathbf{k} - \mathbf{k}_F)$, where \mathbf{k}_F is a vector in the direction of \mathbf{k} and residing on the FS. Following the conventional FL methodology, we divide electron states into “low-energy” (near the Fermi energy) and “high-energy” ones. Effects of the interaction via high-energy states are parameterized by the self-energy $\tilde{\Sigma}_{\mathbf{k}}^R(\omega)$. An expansion of $\tilde{\Sigma}_{\mathbf{k}}^R(\omega)$ near the FS

$$\tilde{\Sigma}_{\mathbf{k}}^R(\omega) = \omega \left(\frac{1}{Z_{\mathbf{k}_F}} - 1 \right) + (\mathbf{u}_{\mathbf{k}_F} - \mathbf{v}_{\mathbf{k}_F}^0) \cdot (\mathbf{k} - \mathbf{k}_F) \quad (2.1)$$

defines the quasiparticle renormalization factor

$$Z_{\mathbf{k}_F} = \left(1 + \frac{\partial \tilde{\Sigma}_{\mathbf{k}_F}^R}{\partial \omega} \Big|_{\omega=0} \right)^{-1} \quad (2.2)$$

and renormalized dispersion $\varepsilon_{\mathbf{k}} = \mathbf{v}_{\mathbf{k}_F} \cdot (\mathbf{k} - \mathbf{k}_F)$ of the low-energy states, where

$$\mathbf{v}_{\mathbf{k}_F} = Z_{\mathbf{k}_F} \mathbf{u}_{\mathbf{k}_F} = Z_{\mathbf{k}_F} \left(\mathbf{v}_{\mathbf{k}_F}^0 - \nabla_{\mathbf{k}} \tilde{\Sigma}_{\mathbf{k}}(0) \Big|_{\mathbf{k}=\mathbf{k}_F} \right). \quad (2.3)$$

(As in I, we define the single-particle self-energy as $G_{\mathbf{k}}^{-1}(\omega, T) = \omega + \Sigma_{\mathbf{k}}(\omega, T) - \varepsilon_{\mathbf{k}}$.) The renormalization factor and both velocities ($\mathbf{v}_{\mathbf{k}_F}$ and $\mathbf{u}_{\mathbf{k}_F}$) are defined at point \mathbf{k}_F of the FS and, in general, vary over the FS. The (Matsubara) Green’s function describing the low-energy electron states is given by

$$G_{\mathbf{k}}^0(\omega_m) = \frac{1}{i\omega_m/Z_{\mathbf{k}_F} - \mathbf{u}_{\mathbf{k}_F} \cdot (\mathbf{k} - \mathbf{k}_F)} = \frac{Z_{\mathbf{k}_F}}{i\omega_m - \varepsilon_{\mathbf{k}}}, \quad (2.4)$$

where $\omega_m = \pi T(2m + 1)$.

The combination of properties formulated above defines the “bare” low-energy theory described by the action

$$\mathcal{S} = T \sum_{\omega_m} \int_{\mathbf{k}} \bar{\psi}_{\omega_m, \mathbf{k}} [i\omega_m/Z_{\mathbf{k}_F} - \mathbf{u}_{\mathbf{k}_F} \cdot (\mathbf{k} - \mathbf{k}_F)] \psi_{\omega_m, \mathbf{k}}, \quad (2.5)$$

where $\int_{\mathbf{k}}$ is a shorthand notation for $\int d^D k / (2\pi)^D$. The residual interaction between low-energy quasiparticles is described by an instantaneous potential $U_{\mathbf{q}}$, which is already dressed up by high-energy states and assumed to be non-singular for any \mathbf{q} that connects two points on the FS, including $\mathbf{q} = 0$. Dynamic screening of the interaction by low-energy states, which gives rise to finite

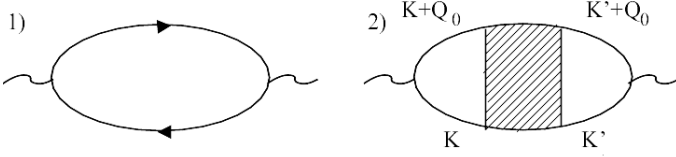


FIG. 1. Diagrams for the current-current correlation function: \mathcal{K}_1 (diagram 1) and \mathcal{K}_2 (diagram 2). The “four-momenta” in diagram 2) are $K = (\omega_m, \mathbf{k})$, $K' = (\omega_{m'}, \mathbf{k}')$, and $Q_0 = (\Omega_n, 0)$. The shaded box is the vertex $\Gamma_{\mathbf{k}\mathbf{k}'}(\omega_m, \omega_{m'}, \Omega_n)$.

lifetime of quasiparticles and hence finite conductivity, is treated explicitly. To avoid double-counting, we assume that mass renormalization is already absorbed into the parameters of the bare theory.

In the presence of an external electromagnetic field described by vector potential \mathcal{A} , the momentum \mathbf{k} in the bare action, Eq. (2.5), is replaced by $\mathbf{k} - e\mathcal{A}/c$. The corresponding current vertex contains the “charge velocity” $\mathbf{u}_{\mathbf{k}_F}$ [Eq. (2.3)]. Note that $\mathbf{u}_{\mathbf{k}_F}$ is renormalized only by the \mathbf{k} dependent part of $\tilde{\Sigma}_{\mathbf{k}}^R(\omega)$,^{5,21} in contrast to the full Fermi velocity $\mathbf{v}_{\mathbf{k}_F}$, which is renormalized both by $\nabla_{\mathbf{k}}\tilde{\Sigma}^R$ and $\partial\tilde{\Sigma}_{\mathbf{k}_F}^R/\partial\omega$.

$$\mathcal{K}_2(\Omega_n, T) = -\frac{2}{D}T^2 \sum_{\omega_m, \omega_{m'}} \int_{\mathbf{k}} \int_{\mathbf{k}'} \mathbf{u}_{\mathbf{k}_F} \cdot \mathbf{u}_{\mathbf{k}'_F} G_{\mathbf{k}}(\omega_m) G_{\mathbf{k}}(\omega_m + \Omega_n) \Gamma_{\mathbf{k}\mathbf{k}'}(\omega_m, \omega_{m'}, \Omega_n) G_{\mathbf{k}'}(\omega_{m'}) G_{\mathbf{k}'}(\omega_{m'} + \Omega_n), \quad (2.8)$$

where the Green’s functions and the vertex part $\Gamma_{\mathbf{k}\mathbf{k}'}(\omega_m, \omega_{m'}, \Omega_n)$ contain the effects of residual interaction between low-energy quasiparticles.

The calculation of diagram 1 in Fig. 1 is fairly straightforward. Replacing the Matsubara sum by a contour integral and converting the momentum integral into integrals over $d\varepsilon_{\mathbf{k}}$ and over the FS element $dA_{\mathbf{k}_F}$, we obtain for the imaginary part of \mathcal{K}_1^R

$$\text{Im}\mathcal{K}_1^R(\Omega, T) = \frac{2}{\pi D(2\pi)^D} \oint dA_{\mathbf{k}_F} \frac{u_{\mathbf{k}_F}^2}{v_{\mathbf{k}_F}} \int d\omega \int d\varepsilon_{\mathbf{k}} \times [n_F(\omega) - n_F(\omega + \Omega)] \text{Im}G_{\mathbf{k}}^R(\omega) \text{Im}G_{\mathbf{k}}^R(\omega + \Omega), \quad (2.9)$$

where $n_F(\epsilon)$ is the Fermi function, $G_{\mathbf{k}}^{R,A}(\omega) = Z_{\mathbf{k}_F}/[\omega - \varepsilon_{\mathbf{k}} \pm iZ_{\mathbf{k}_F} \text{Im}\Sigma_{\mathbf{k}}^R(\omega)]$, and $\text{Im}\Sigma_{\mathbf{k}}^R(\omega)$ accounts for the residual interaction.

2. Canonical Fermi liquids

In this Section, we restrict the analysis to conventional FLs. (We will show later, in Sec. II A 3, that the result for the conductivity applies to non-conventional FLs as well). For a conventional FL on the lattice, $\text{Im}\Sigma_{\mathbf{k}_F}^R(\omega, T)$ is still

To simplify notations, we assume that a metal has cubic symmetry, in which case the conductivity tensor reduces to $\sigma_{ij} = \delta_{ij}\sigma$. The diagonal component of the conductivity is given by the Kubo formula

$$\sigma(\Omega, T) = \frac{e^2}{i\Omega} [\mathcal{K}^R(\Omega, T) + \mathcal{K}^{\text{dia}}(T)], \quad (2.6)$$

where $\mathcal{K}^R(\Omega, T) = \mathcal{K}_1^R(\Omega, T) + \mathcal{K}_2^R(\Omega, T)$ is the retarded current-current correlation function, represented by a sum of two diagrams in Fig. 1, and $(e^2/i\Omega)\mathcal{K}^{\text{dia}}(T)$ is the diamagnetic part of the conductivity, which cancels the $\Omega = 0$ term in $\mathcal{K}^R(\Omega, T)$ [the sum $\mathcal{K}^R(0, T) + \mathcal{K}^{\text{dia}}(T)$ must vanish for a normal metal by gauge invariance]. In what follows, we assume that the $\Omega = 0$ piece is already subtracted from $\mathcal{K}^R(\Omega, T)$ and do not specify an explicit form of \mathcal{K}^{dia} .

On the Matsubara axis, the diagrams in Fig. 1 are given by

$$\mathcal{K}_1(\Omega_n, T) = -\frac{2}{D}T \sum_{\omega_m} \int_{\mathbf{k}} u_{\mathbf{k}_F}^2 G_{\mathbf{k}}(\omega_m) G_{\mathbf{k}}(\omega_m + \Omega_n) \quad (2.7)$$

and

given by Eq. (1.1) with the only proviso that the prefactor now varies along the FS: $C \rightarrow C_{\mathbf{k}_F}$. The dependence of $\text{Im}\Sigma_{\mathbf{k}_k}^R(\omega, T)$ on $\varepsilon_{\mathbf{k}}$ is weak and can be neglected. The integral over $\varepsilon_{\mathbf{k}}$ is then solved readily:

$$\int d\varepsilon_{\mathbf{k}} \text{Im}G_{\mathbf{k}}^R(\omega) \text{Im}G_{\mathbf{k}}^R(\omega + \Omega) = \pi Z_{\mathbf{k}_F} \text{Im} [\Omega/Z_{\mathbf{k}_F} + i\text{Im}\Sigma_{\mathbf{k}_F}^R(\omega, T) + i\text{Im}\Sigma_{\mathbf{k}_F}^R(\omega + \Omega, T)]^{-1}. \quad (2.10)$$

The high-frequency regime is defined by the condition

$$\Omega \gg Z_{\mathbf{k}_F} \text{Im}\Sigma_{\mathbf{k}_F}(\Omega, T). \quad (2.11)$$

For a conventional FL, this condition implies that $\Omega \gg C_{\mathbf{k}_F} \max\{\Omega^2, T^2\}$ for all points on the FS. The relation between Ω and T is arbitrary but we do assume that $\Omega, T \ll E_F$. In this regime, Eq. (2.10) is expanded in the imaginary parts of the self-energies and their sum is averaged with the difference of the Fermi functions. For

a conventional FL, the last step amounts to

$$\begin{aligned} & \int_{-\infty}^{\infty} d\omega [n_F(\omega) - n_F(\omega + \Omega)] [\text{Im}\Sigma_{\mathbf{k}_F}^R(\omega) + \text{Im}\Sigma_{\mathbf{k}_F}^R(\omega + \Omega)] \\ &= C_{\mathbf{k}_F} \int_{-\infty}^{\infty} d\omega [n_F(\omega) - n_F(\omega + \Omega)] [\omega^2 + (\omega + \Omega)^2 + 2(\pi T)^2] \\ &= \frac{2}{3} C_{\mathbf{k}_F} \Omega (\Omega^2 + 4\pi^2 T^2). \end{aligned} \quad (2.12)$$

It is at this step when the difference between the coefficients of the T^2 parts in $\text{Im}\Sigma_{\mathbf{k}_F}^R$ and σ occurs. Using (2.12), we obtain

$$\text{Re}\sigma_1(\Omega, T) = \frac{e^2}{\Omega} \text{Im}\mathcal{K}_1^R(\Omega, T) = B_1 \frac{\Omega^2 + 4\pi^2 T^2}{\Omega^2} \quad (2.13)$$

with $B_1 = (4e^2/3D(2\pi)^D) \oint dA_{\mathbf{k}_F} (u_{\mathbf{k}_F}^2/v_{\mathbf{k}_F}) Z_{\mathbf{k}_F}^3 C_{\mathbf{k}_F}$. In the high-frequency regime, $\text{Re}\sigma \ll \text{Im}\sigma = \omega_p^2/4\pi\Omega$, where ω_p is the effective plasma frequency. Expanding $\rho(\Omega, T) = 1/\sigma(\Omega, T)$ in $\text{Re}\sigma/\text{Im}\sigma$, we obtain Eq. (1.2) with prefactor $A' = (4\pi)^2 B_1/\omega_p^4$.

To analyze the contribution of the vertex corrections represented by diagram 2 in Fig. 1, we perform analytic continuation of $\mathcal{K}_2(\Omega_n, T)$, following the procedure developed by Eliashberg.⁵ The resulting expression is quite involved but to find the real part the conductivity we need only that part of $\mathcal{K}_2^R(\Omega, T)$ which contains the product of the retarded and advanced Green's functions located on the same side relative to the vertex. Only such products will survive upon integrating over $\varepsilon_{\mathbf{k}}$ and $\varepsilon_{\mathbf{k}'}$. In general, $\mathcal{K}_2^R(\Omega, T)$ contains vertices which are obtained by analytically continuing the Matsubara vertex $\Gamma_{\mathbf{k}\mathbf{k}'}(\omega_m, \omega_{m'}, \Omega_n)$ via the following relations: $i\omega_m = \omega + i\text{Im}\omega$, $i\omega_{m'} = \omega' + i\text{Im}\omega'$, and $i\Omega_n = \Omega + i\text{Im}\Omega$, where all the imaginary parts are infinitesimally small. Analytic properties of continued vertices are determined by relations between the imaginary parts of the three frequencies. The part of $\mathcal{K}_2^R(\Omega, T)$ that we are interested in contains vertices $\Gamma_{\mathbf{k}\mathbf{k}'}^{\text{II-IV}}(\omega, \omega', \Omega)$, where Roman numerals indicate regions in the $(\text{Im}\omega, \text{Im}\omega')$ plane, as shown in Fig. 3 (for definiteness, we set $\text{Im}\Omega > 0$). Explicitly,

$$\mathcal{K}_2^R(\Omega, T) = \frac{1}{4\pi^2 D} \int_{\mathbf{k}} \int_{\mathbf{k}'} \mathbf{u}_{\mathbf{k}_F} \cdot \mathbf{u}_{\mathbf{k}'_F} \int d\omega \int d\omega' [n_F(\omega) - n_F(\omega + \Omega)] G_{\mathbf{k}}^R(\omega + \Omega) G_{\mathbf{k}}^A(\omega) \Gamma_{\mathbf{k}\mathbf{k}'}(\omega, \omega', \Omega) G_{\mathbf{k}'}^R(\omega' + \Omega) G_{\mathbf{k}'}^A(\omega'), \quad (2.14)$$

where

$$\Gamma_{\mathbf{k}\mathbf{k}'} = \coth \frac{\omega' - \omega}{2T} (\Gamma_{\mathbf{k}\mathbf{k}'}^{\text{II}} - \Gamma_{\mathbf{k}\mathbf{k}'}^{\text{III}}) + \coth \frac{\omega + \omega' + \Omega}{2T} (\Gamma_{\mathbf{k}\mathbf{k}'}^{\text{III}} - \Gamma_{\mathbf{k}\mathbf{k}'}^{\text{IV}}) - \tanh \frac{\omega'}{2T} \Gamma_{\mathbf{k}\mathbf{k}'}^{\text{II}} + \tanh \frac{\omega' + \Omega}{2T} \Gamma_{\mathbf{k}\mathbf{k}'}^{\text{IV}}. \quad (2.15)$$

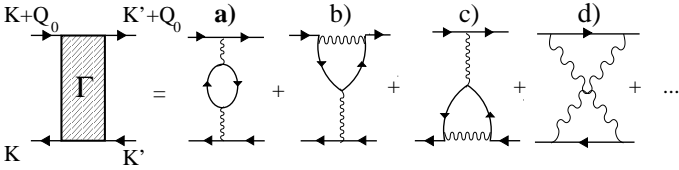


FIG. 2. Lowest order diagrams for the vertex in diagram 2) of Fig. 1.

[For brevity, we do not spell out the arguments ω, ω', Ω which are the same in all vertices in Eq. (2.15).]

Equations (2.15) and (2.14) allow one to extract the Ω and T dependences for any vertex diagram. For example, vertex diagram *a* in Fig. 2 reads

$$\Gamma_{\mathbf{k}\mathbf{k}'}^{\{a\}}(\omega_m, \omega_{m'}, \Omega_n) = U_{\mathbf{k}-\mathbf{k}'}^2 \Pi_{\mathbf{k}-\mathbf{k}'}(\omega_m - \omega_{m'}), \quad (2.16)$$

where $\Pi_{\mathbf{q}}(\epsilon)$ is the polarization bubble. Continuing this expression to real frequencies, we obtain $\Gamma_{\mathbf{k}\mathbf{k}'}^{a, \text{II}} = U_{\mathbf{k}-\mathbf{k}'}^2 \Pi_{\mathbf{k}-\mathbf{k}'}^R(\omega - \omega')$ in region II, where $\text{Im}(\omega - \omega') > 0$, and $\Gamma_{\mathbf{k}\mathbf{k}'}^{a, \text{III}} = \Gamma_{\mathbf{k}\mathbf{k}'}^{a, \text{IV}} = U_{\mathbf{k}-\mathbf{k}'}^2 \Pi_{\mathbf{k}-\mathbf{k}'}^A(\omega - \omega') = U_{\mathbf{k}-\mathbf{k}'} \mathbf{q}^2 [\Pi_{\mathbf{k}-\mathbf{k}'}^R(\omega - \omega')]^*$ in regions III and IV, where $\text{Im}(\omega - \omega') < 0$. Combining the contributions from regions II-IV, we obtain

$$\Gamma_{\mathbf{k}\mathbf{k}'}^{\{a\}} = U_{\mathbf{k}-\mathbf{k}'}^2 \{ 2\text{Re}\Pi_{\mathbf{k}-\mathbf{k}'}^R(\omega - \omega') [n_F(\omega') - n_F(\omega' + \Omega)] + 2i\text{Im}\Pi_{\mathbf{k}-\mathbf{k}'}^R(\omega - \omega') [2n_B(\omega' - \omega) + n_F(\omega') + n_F(\omega' + \Omega)] \}, \quad (2.17)$$

where $n_B(\epsilon)$ is a Bose function.

As before, we replace each of the two momentum integrals in Eq. (2.14) by integrals over the Fermi surface

and over the dispersion, and set $\mathbf{k} = \mathbf{k}_F$ and $\mathbf{k}' = \mathbf{k}'_F$ everywhere except for the Green's functions. In the high-frequency regime, the Green's functions in Eq. (2.14) can

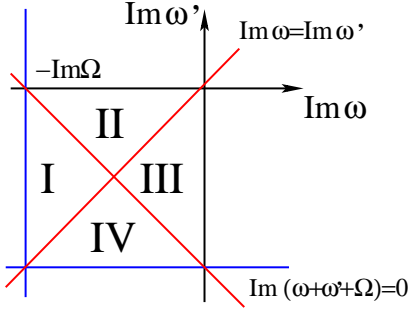


FIG. 3. (color on-line). Regions of the $(\text{Im}\omega, \text{Im}\omega')$ plane.

be replaced by the bare ones [Eq. (2.4)]; then the product $\int d\varepsilon_{\mathbf{k}} G_{\mathbf{k}}^R(\omega + \Omega) G_{\mathbf{k}}^A(\omega) \int d\varepsilon_{\mathbf{k}'} G_{\mathbf{k}'}^R(\omega' + \Omega) G_{\mathbf{k}'}^A(\omega') = -4\pi^2 Z_{\mathbf{k}_F}^2 Z_{\mathbf{k}'_F}^2 / \Omega^2$ is real. Therefore, the imaginary part of the current-current correlator is given by $\text{Im}\Gamma_{\mathbf{k}\mathbf{k}'}^{\{a\}}$ from Eq. (2.17). Recalling that $\text{Im}\Pi_{\mathbf{q}}(\Omega) = -\mathcal{D}_{\mathbf{q}}\Omega$, where

$$D_{\mathbf{q}} = \frac{1}{(2\pi)^2} \oint \frac{dA_{\mathbf{k}'_F}}{v_{\mathbf{k}'_F}} Z_{\mathbf{k}'_F} Z_{\mathbf{k}'_F + \mathbf{q}} \delta(\varepsilon_{\mathbf{k}'_F + \mathbf{q}}) \Big|_{\varepsilon_{\mathbf{k}'_F} = 0} \quad (2.18)$$

(cf. Eq. (2.7) of I), and relabeling $\omega' \rightarrow \omega + \Omega'$, we obtain the contribution of diagram *a* to the conductivity

$$\text{Re}\sigma_2^{\{a\}} = \frac{8\pi^2 e^2}{(2\pi)^D} \oint dA_{\mathbf{k}_F} \oint dA_{\mathbf{k}'_F} \int d\omega \int d\Omega' \mathcal{N}(\omega, \Omega', \Omega) \times \frac{\mathbf{u}_{\mathbf{k}_F} \cdot \mathbf{u}_{\mathbf{k}'_F}}{v_{\mathbf{k}_F} v_{\mathbf{k}'_F}} Z_{\mathbf{k}_F}^2 Z_{\mathbf{k}'_F}^2 \mathcal{D}_{\mathbf{k}_F - \mathbf{k}'_F} U_{\mathbf{k}_F - \mathbf{k}'_F}^2, \quad (2.19)$$

where

$$\mathcal{N}(\omega, \Omega', \Omega) = \frac{\Omega'}{\Omega^3} [n_F(\omega) - n_F(\omega + \Omega)] \times [2n_B(\Omega') + n_F(\omega + \Omega') + n_F(\omega + \Omega' + \Omega)]. \quad (2.20)$$

$$\Gamma_{\mathbf{k}\mathbf{k}'}^{\{d\}} = 2\text{Re}\mathcal{C}_{\mathbf{k}\mathbf{k}'}^R(\omega, \omega', \Omega) [n_F(\omega') - n_F(\omega' + \Omega)] + 2i\text{Im}\mathcal{C}_{\mathbf{k}\mathbf{k}'}^R(\omega, \omega', \Omega) [2n_B(\omega' + \omega + \Omega) + n_F(\omega') + n_F(\omega' + \Omega)]. \quad (2.23)$$

As before, we need only the imaginary part of the vertex which contains

$$\text{Im}\mathcal{C}_{\mathbf{k}\mathbf{k}'}^R = \int_{\mathbf{p}} \int \frac{d\varepsilon}{\pi} \text{Im}G_{\mathbf{p}}^R(\varepsilon) \text{Im}G_{\mathbf{k} + \mathbf{k}' - \mathbf{p}}^R(\omega + \omega' + \Omega - \varepsilon) \times \tanh \frac{\varepsilon}{2T} U_{\mathbf{k} - \mathbf{p}} U_{\mathbf{p} - \mathbf{k}'}. \quad (2.24)$$

[For $U_{\mathbf{k}} = \text{const}$, \mathcal{C} reduces to a Cooper bubble.] Substituting explicit expressions for the spectral functions and integrating over ε and $\varepsilon_{\mathbf{p}}$, we obtain $\text{Im}\mathcal{C}_{\mathbf{k}\mathbf{k}'}^R = \mathcal{C}_0(\omega + \omega' + \Omega)$ in the low-frequency limit, where \mathcal{C}_0 contains a product of two interactions averaged over the

The integral over Ω' in Eq. (2.19) is the same as in the sum of the imaginary parts of the self-energies corresponding to diagram *a* in Fig. 1 of I [cf. Eq. (2.5a) in I]. This integral gives $\frac{1}{2}(\omega^2 + (\omega + \Omega)^2 + 2\pi^2 T^2)$. Averaging the last result with the difference of the Fermi functions, as in Eq. (2.12), we obtain

$$\int d\omega \int d\Omega' \mathcal{N}(\omega, \Omega', \Omega) = \frac{1}{3} \frac{\Omega^2 + 4\pi^2 T^2}{\Omega^2}. \quad (2.21)$$

Thus $\text{Re}\sigma_2^{\{a\}}$ differs from $\text{Re}\sigma_1$ in Eq. (2.13) only by a prefactor, which can be read off from Eq. (2.19).

Other diagrams for $\mathcal{K}_2^R(\Omega, T)$ can be analyzed in a similar fashion. For example, diagrams *b* and *c* in Fig. 2 are similar to diagram *a* with the only difference that $U_{\mathbf{k} - \mathbf{k}'}^2 \text{Im}\Pi_{\mathbf{k} - \mathbf{k}'}^R(\omega - \omega')$ in Eq. (2.17) is replaced by $U_{\mathbf{k} - \mathbf{k}'} \text{Im}\mathcal{P}_{\mathbf{k}, \mathbf{k}'}^R(\omega' - \omega)$, where

$$\text{Im}\mathcal{P}_{\mathbf{k}, \mathbf{k}'}^R(\Omega) = \int d\varepsilon [n_F(\varepsilon) - n_F(\varepsilon + \Omega)] \times \int_{\mathbf{p}} \text{Im}G_{\mathbf{p}}(\varepsilon) \text{Im}G_{\mathbf{p} + \mathbf{k}' - \mathbf{k}}(\varepsilon + \Omega) U_{\mathbf{k} - \mathbf{p}}. \quad (2.22)$$

In I, we showed that the analytic properties of \mathcal{P}^R in the frequency plane are the same as those of the polarization bubble. Therefore, the contributions of diagrams *b* and *c* to $\text{Re}\sigma$, which are equal to each other, also scale as $(\Omega^2 + 4\pi^2 T^2)/\Omega^2$ with a prefactor different from that of diagram *a*. [For $U_{\mathbf{q}} = \text{const}$, the combined contribution of *b* and *c* cancels that of *a*.]

The Cooper-channel vertex—diagram *d*—appears to be somewhat different from particle-hole diagrams *a-c* but, in fact, it gives the same result. To see this, we notice that the Matsubara vertex in diagram *d* depends only on the combination $\omega_m + \omega_{m'} + \Omega_n$; hence, analytic properties of the retarded vertex depend on whether one is above or below the $\text{Im}\omega + \text{Im}\omega' + \text{Im}\Omega = 0$ line in Fig. 3. Therefore, $\Gamma_{\mathbf{k}\mathbf{k}'}^{\text{II}} = \Gamma_{\mathbf{k}\mathbf{k}'}^{\text{III}} = (\Gamma_{\mathbf{k}\mathbf{k}'}^{\text{IV}})^*$, and the vertex reduces

FS. Substituting this result into the imaginary part of Eq. (2.23), and relabeling $\omega \rightarrow -\omega$ and $\omega + \omega' + \Omega \rightarrow \Omega'$, we again arrive at the same integral as in Eq. (2.21).

The recipe for extracting the $\Omega^2 + 4\pi^2 T^2$ scaling form of $\text{Re}\rho$ from a diagram of arbitrary order is now clear: one needs to extract a factor of Ω from either a particle-hole or particle-particle convolutions of the Green's functions in the vertex, integrate it with the combination of the Fermi and Bose functions in Eq. (2.20), and then average the result with the difference of the Fermi function. Up to a prefactor, all diagrams produce the same Ω/T scaling form of $\text{Re}\rho$ given by Eq. (1.2). As it was the case

with the self-energy considered in I, the overall prefactor cannot be expressed in a compact form.

3. Non-canonical Fermi liquids

The analysis of the preceding section was limited to the case of a conventional FL, when the infrared singularity arising from the Ω/q scaling of the polarization bubble is suppressed by the phase space volume, and each of the diagram considered above is convergent on its own. In $D \leq 2$, the phase space is too small to suppress the singularities and the self-energy scales with ω in a non-canonical way: as $\omega^2 \ln |\omega|$ in $D = 2$ and as $|\omega|^D$ in $1 < D < 2$. However, infrared singularities in different diagrams for the conductivity cancel each other. This cancellation manifests the gauge-invariance of the conductivity. In perhaps more familiar terms, this effect makes the conductivity to depend on the transport rather than single-particle relaxation time. It is more convenient to see this effect in the Boltzmann equation, where the electron-electron contribution to the conductivity is expressed via a change in the electron current carried by two electrons before and after a collision:^{17,18} $(\Delta \mathbf{v})^2 \equiv \langle (\mathbf{v}_{\mathbf{k}} + \mathbf{v}_{\mathbf{p}} - \mathbf{v}_{\mathbf{k}-\mathbf{q}} - \mathbf{v}_{\mathbf{p}+\mathbf{q}})^2 \rangle$, where $\langle \dots \rangle$ stands for averaging over the FS. For $q \rightarrow 0$, $(\Delta \mathbf{v})^2$ vanishes as q^2 , which suppresses the infrared singularity for $D > 1$.

To see how the same cancellation occurs in the Kubo formula, we consider two diagrams: diagram 1 in Fig. 1 with both Green's functions dressed by a single-bubble self-energy correction (diagram *a* in Fig. 1 of I) and diagram 2 in Fig. 1 with vertex correction *a* in Fig. 2. As we are interested in the $q = 0$ limit, it is convenient to decompose the momentum transfer \mathbf{q} into components along and perpendicular to the local Fermi velocity: $\mathbf{q} =$

$q_{\parallel} \hat{\mathbf{v}}_{\mathbf{k}} + \mathbf{q}_{\perp}$, where $\hat{\mathbf{v}}_{\mathbf{k}} = \mathbf{v}_{\mathbf{k}}/v_{\mathbf{k}}$, $q_{\parallel} \ll q_{\perp} \ll \bar{k}_F$, and \bar{k}_F is the characteristic ‘‘radius’’ of the FS. Accordingly, the (renormalized) dispersion is expanded as

$$\varepsilon_{\mathbf{k}+\mathbf{q}} = \varepsilon_{\mathbf{k}} + v_{\mathbf{k}} q_{\parallel} + q_{\perp}^2/2m_{\mathbf{k}}, \quad (2.25)$$

where $m_{\mathbf{k}}$ measures the local curvature of the FS. The imaginary part of the self-energy insertions into diagram 1 of Fig. 1) is given by [cf. I, Eq. (2.5a)]

$$\text{Im} \Sigma_{\mathbf{k}}^{R,a}(\omega, T) = \int_{\mathbf{q}} U_{\mathbf{q}}^2 \int \frac{d\Omega}{\pi} [n_B(\Omega) + n_F(\omega + \Omega)] \times \text{Im} G_{\mathbf{k}+\mathbf{q}}^R(\omega + \Omega) \text{Im} \Pi_{\mathbf{q}}^R(\Omega), \quad (2.26)$$

where, as before, $\text{Im} \Pi_{\mathbf{q}}^R(\Omega) = -\mathcal{D}_{\mathbf{q}} \Omega$ and $\mathcal{D}_{\mathbf{q}} \propto 1/q$ as $q \rightarrow 0$. We neglect q_{\parallel} everywhere but in $\text{Im} G_{\mathbf{k}+\mathbf{q}}^R(\omega + \Omega)$, integrate over q_{\parallel} , and substitute the result into Eq. (2.9), which is then expanded in $\text{Im} \Sigma^R$. This yields

$$\text{Im} \mathcal{K}_1^R(\Omega, T) = \frac{\Omega}{\pi D} \int \frac{dA_{\mathbf{k}_F}}{(2\pi)^D} \frac{u_{\mathbf{k}_F}^2}{v_{\mathbf{k}_F}^2} Z_{\mathbf{k}_F}^3 \int d\omega \int d\Omega' \mathcal{N}(\omega, \Omega', \Omega) \times \int \frac{d^{D-1} q_{\perp}}{(2\pi)^{D-1}} \mathcal{D}_{\mathbf{q}_{\perp}} U_{\mathbf{q}_{\perp}}^2 Z_{\mathbf{k}_F+\mathbf{q}_{\perp}}, \quad (2.27)$$

where \mathcal{N} is given by Eq. (2.20). In $D \leq 2$, the \mathbf{q}_{\perp} integral is Eq. (2.27) infrared divergent. However, this divergence is canceled by vertex part *a* in Fig. 2. To see this cancellation, we need to assume that not only the charge velocity, defined by Eq. (2.3), but also its derivative on the FS is known. Then, relabeling $\mathbf{k}' = \mathbf{k} + \mathbf{q}$ in Eq. (2.14), we expand $\mathbf{u}_{\mathbf{k}+\mathbf{q}}$ as

$$\mathbf{u}_{\mathbf{k}+\mathbf{q}} = \mathbf{u}_{\mathbf{k}} + ([\hat{\mathbf{v}}_{\mathbf{k}} q_{\parallel} + \mathbf{q}_{\perp}] \cdot \nabla) \mathbf{u}_{\mathbf{k}}. \quad (2.28)$$

Substituting this expansion into Eq. (2.14) with $\Gamma = \Gamma^{\{a\}}$, we obtain

$$\text{Im} \mathcal{K}_{2a}^R(\Omega, T) = \frac{\Omega}{2\pi^2 D} \int \frac{dA_{\mathbf{k}_F}}{(2\pi)^D v_{\mathbf{k}_F}} \int d\varepsilon_{\mathbf{k}} \int \frac{dq_{\parallel}}{2\pi} \int \frac{d^{D-1} q_{\perp}}{(2\pi)^{D-1}} \int d\omega \int d\Omega' \mathbf{u}_{\mathbf{k}_F} \cdot (\mathbf{u}_{\mathbf{k}_F} + ([\hat{\mathbf{v}}_{\mathbf{k}} q_{\parallel} + \mathbf{q}_{\perp}] \cdot \nabla) \mathbf{u}_{\mathbf{k}} |_{\mathbf{k}=\mathbf{k}_F}) \times G_{\mathbf{k}}^R(\omega + \Omega) G_{\mathbf{k}}^A(\omega) G_{\mathbf{k}+\mathbf{q}}^R(\omega + \Omega' + \Omega) G_{\mathbf{k}+\mathbf{q}}^A(\omega + \Omega') U_{\mathbf{q}}^2 \mathcal{D}_{\mathbf{q}} \mathcal{N}(\omega, \Omega', \Omega). \quad (2.29)$$

First, we integrate the product $G_{\mathbf{k}+\mathbf{q}}^R G_{\mathbf{k}+\mathbf{q}}^A \mathbf{u}_{\mathbf{k}+\mathbf{q}}$ over q_{\parallel} , setting $q_{\parallel} = 0$ everywhere else in the integrand. The q_{\parallel} independent and linear-in- q_{\parallel} terms in $\mathbf{u}_{\mathbf{k}+\mathbf{q}}$ produce two integrals

$$\int \frac{dq_{\parallel}}{2\pi} \left(\frac{1}{q_{\parallel}} \right) G_{\mathbf{k}+\mathbf{q}}^R(\omega' + \Omega) G_{\mathbf{k}+\mathbf{q}}^A(\omega') = \left(\frac{i Z_{\mathbf{k}_F+\mathbf{q}_{\perp}}^2}{v_{\mathbf{k}} \Omega} - \frac{Z_{\mathbf{k}_F+\mathbf{q}_{\perp}}^2}{i v_{\mathbf{k}}^2 \Omega} \frac{q_{\perp}^2}{2m_{\mathbf{k}}} \right), \quad (2.30)$$

where terms of order Ω, T were neglected compared to $q_{\perp}^2/2m_{\mathbf{k}}$ in the second line. Next, we integrate $G_{\mathbf{k}}^R G_{\mathbf{k}}^A$ over $\varepsilon_{\mathbf{k}}$, setting $\varepsilon_{\mathbf{k}} = 0$ everywhere else in the integrand.

The term proportional to \mathbf{q}_{\perp} vanishes by symmetry, and we obtain

$$\text{Im} \mathcal{K}_{2a}^R(\Omega) = -\frac{\Omega}{\pi D} \oint \frac{dA_{\mathbf{k}_F}}{(2\pi)^D} \int d\omega \int d\Omega' \mathcal{N}(\omega, \Omega', \Omega) \times \frac{\mathbf{u}_{\mathbf{k}_F} \cdot \mathbf{w}_{\mathbf{k}_F}}{v_{\mathbf{k}}^2} Z_{\mathbf{k}_F}^2, \quad (2.31)$$

where

$$\mathbf{w}_{\mathbf{k}_F} = \int \frac{d^{D-1} q_{\perp}}{(2\pi)^{D-1}} \left[\mathbf{u}_{\mathbf{k}_F} - \frac{q_{\perp}^2}{2m_{\mathbf{k}_F} v_{\mathbf{k}_F}} (\hat{\mathbf{v}}_{\mathbf{k}} \cdot \nabla_{\mathbf{k}}) \mathbf{u}_{\mathbf{k}} |_{\mathbf{k}=\mathbf{k}_F} \right] \times \mathcal{D}_{\mathbf{q}_{\perp}} U_{\mathbf{q}_{\perp}}^2 Z_{\mathbf{k}_F+\mathbf{q}_{\perp}}^2. \quad (2.32)$$

The sum of two contributions to $\text{Im}\mathcal{K}$, i.e., Eqs. (2.27) and (2.31), contains a combination

$$\int \frac{dA_{\mathbf{k}_F}}{v_{\mathbf{k}_F}^2} Z_{\mathbf{k}_F}^2 Z_{\mathbf{k}_F+\mathbf{q}} \left[u_{\mathbf{k}_F}^2 (Z_{\mathbf{k}_F} - Z_{\mathbf{k}_F+\mathbf{q}_\perp}) \right. \quad (2.33)$$

$$\left. + \frac{q_\perp^2}{2m_{\mathbf{k}_F} v_{\mathbf{k}_F}} \mathbf{u}_{\mathbf{k}_F} \cdot (\hat{\mathbf{v}}_{\mathbf{k}} \cdot \nabla_{\mathbf{k}}) \mathbf{u}_{\mathbf{k}} \Big|_{\mathbf{k}=\mathbf{k}_F} Z_{\mathbf{k}_F+\mathbf{q}_\perp} \right],$$

which vanishes as q_\perp^2 for $q_\perp \rightarrow 0$ and thus suppresses the $1/q_\perp$ divergence for all $D > 0$. Therefore, the optical resistivity in the high-frequency regime has the same $\Omega^2 + 4\pi^2 T^2$ form both in conventional and non-conventional FLs. Notice that the other transport coefficients behave differently in these two cases; for example, the dc thermal conductivity of a 2D FL behaves as $1/T \ln T$, as opposed to the $1/T$ behavior in 3D.²⁴

B. Bosonic first-Matsubara-frequency rule

Just as it was the case for a single-particle self-energy considered in I, the $\Omega^2 + 4\pi^2 T^2$ scaling form of the optical resistivity can be related to the analytic properties of the current-current correlator along the Matsubara axis.

First, we consider the Matsubara version of diagram 1 in Fig. 1, given by Eq. (2.9). Recalling that $\text{sgn}\Sigma_{\mathbf{k}_F}(\omega_m) = \text{sgn}\omega_m$, we integrate over $\varepsilon_{\mathbf{k}}$ to obtain (for $\Omega_n > 0$)

$$\mathcal{K}_1(\Omega_n, T) = -\frac{2iT}{D(2\pi)^{D-1}} \oint dA_{\mathbf{k}_F} \frac{u_{\mathbf{k}_F}^2}{v_{\mathbf{k}_F}} \quad (2.34)$$

$$\times \sum_{\omega_m=-\Omega_n+\pi T}^{\omega_m=-\pi T} \frac{1}{\frac{i\Omega_n}{Z_{\mathbf{k}_F}} + \Sigma_{\mathbf{k}_F}(\omega_m + \Omega_n) + \Sigma_{\mathbf{k}_F}(\omega_m)}.$$

For $\Omega_n = 2\pi T$, only one term with $\omega_m = -\pi T$ survives in the sum

$$\mathcal{K}_1(2\pi T, T) = -\frac{2iT}{D(2\pi)^{D-1}} \oint dA_{\mathbf{k}_F} \frac{u_{\mathbf{k}_F}^2}{v_{\mathbf{k}_F}} \quad (2.35)$$

$$\times \frac{1}{\frac{2\pi iT}{Z_{\mathbf{k}_F}} + \Sigma_{\mathbf{k}_F}(\pi T) + \Sigma_{\mathbf{k}_F}(-\pi T)}.$$

Since the single-particle self-energy satisfies the first (fermionic) Matsubara frequency rule, i.e., $\Sigma_{\mathbf{k}_F}(\pi T) = \Sigma_{\mathbf{k}_F}(-\pi T) = 0 + \mathcal{O}(T^D)$, the residual interaction drops out from $\mathcal{K}_1(2\pi T, T)$ (to order T^3). Consequently, $\text{Im}\mathcal{K}_1^R(\Omega, T)$ vanishes (again, up to $\mathcal{O}(T^D)$ terms), when continued to the first non-zero bosonic Matsubara-frequency $2\pi iT$.

Next, we integrate over $\varepsilon_{\mathbf{k}}$ and $\varepsilon_{\mathbf{k}'}$ as over independent variables in the Matsubara version of the vertex part, Eq. (2.8), setting $\varepsilon_{\mathbf{k}} = \varepsilon_{\mathbf{k}'} = 0$ in the rest of the integrand. At $\Omega = 2\pi T$, only the $\omega_m = \omega_{m'} = -\pi T$ terms survive in the fermionic Matsubara sums and, as before, the fermionic self-energies, evaluated at $\pm\pi T$, drop out.

Therefore,

$$\mathcal{K}_2(2\pi T, T) = -\frac{2}{D(2\pi)^D} \oint dA_{\mathbf{k}_F} \oint dA_{\mathbf{k}'_F} \frac{\mathbf{u}_{\mathbf{k}_F} \cdot \mathbf{u}_{\mathbf{k}'_F}}{v_{\mathbf{k}_F} v_{\mathbf{k}'_F}} \quad (2.36)$$

$$\times Z_{\mathbf{k}_F}^2 Z_{\mathbf{k}'_F}^2 \Gamma_{\mathbf{k}_F, \mathbf{k}'_F}(-\pi T, -\pi T, 2\pi T).$$

Particle-hole diagrams for $\Gamma_{\mathbf{k}, \mathbf{k}'}(\omega_m, \omega_{m'}, \Omega_n)$, e.g., diagrams *a-c* in Fig. 2, depend on $\omega_m - \omega_{m'}$, while particle-particle diagrams, e.g., diagram *d*, depend on $\omega_m + \omega_{m'} + \Omega_n$. Since both combinations of the frequencies vanish at $\omega_m = \omega_{m'} = -\pi T$ and $\Omega_n = 2\pi T$, the vertex in Eq. (2.36) is *static*, i.e., it does not contribute to the real part of the conductivity. Therefore, the vertex-part contribution to $\text{Im}\mathcal{K}^R(\Omega, T)$ vanishes as $\Omega = 2\pi iT$ as well.

Strictly speaking, the proof presented above is valid only for conventional FLs, because the single-particle self-energy obeys the fermionic first-Matsubara-frequency rule only in this case. However, as it was the case in Sec. II A 3, deviations from the canonical behavior caused by infrared singularities must cancel between different diagrams. We did not attempt to repeat the proof for non-conventional FLs because the final result, applicable to both conventional and non-conventional FLs, clearly shows that $\text{Re}\sigma$ vanishes at $\Omega = 2\pi iT$.

III. KUBO FORMULA: ZERO-BUBBLE APPROXIMATION

A. High-frequency regime

Having shown that all diagrams for the conductivity produce the same scaling form in the high-frequency regime, we now consider the case of lower frequencies, when $\Omega \lesssim Z_{\mathbf{k}_F} \Sigma_{\mathbf{k}_F}(\Omega, T)$. The full analysis of the Kubo formula in this regime is rather involved. We will simplify our task and focus on diagram 1 in Fig. 1 which does not include vertex corrections. Although such an approximation can be rigorously justified only in a few special cases, e.g., in the $D = \infty$ limit of the Hubbard model,¹⁶ or when electron-electron scattering connects points of FS with mutually perpendicular Fermi velocities,²² it provides a convenient way to describe a crossover between high- and low-frequency regimes. We also adopt a slightly different version of the FL theory, compared to that considered in the preceding part of the paper. Namely, we assume that the self-energy is isotropic and local, i.e., that it depends on ω much stronger than on $k - k_F$, and include the effects of interactions at all energy scales into the self-energy which, to order ω^2, T^2 is now given by $\Sigma^R(\omega, T) = \omega(1 + \lambda) + iC(\omega^2 + \pi^2 T^2)$. (Since we neglected the variation of the self-energy over the Fermi surface, the subscript \mathbf{k}_F will be suppressed from now on.) Since this model accounts for effects on interaction at all energy scales, the charge and Fermi velocities entering the conductivity diagram coincide with the bare Fermi velocity: $\mathbf{u}_{\mathbf{k}_F} = \mathbf{v}_{\mathbf{k}_F} = \mathbf{v}_{\mathbf{k}_F}^0$. Integrating over the bare dispersion, $\varepsilon_{\mathbf{k}}^0$, we obtain for the conductivity given

by diagram 1

$$\sigma_1(\Omega, T) = \frac{i\omega_{p0}^2}{4\pi\Omega} \int_{-\infty}^{\infty} d\omega \frac{n_F(\omega - \Omega) - n_F(\omega)}{\Omega + \Sigma^R(\omega, T) + \Sigma^R(\Omega - \omega, T)}, \quad (3.1)$$

where the bare plasma frequency is given by

$$\frac{\omega_{p0}^2}{4\pi} = \frac{2e^2}{D(2\pi)^D} \oint dA_{\mathbf{k}_F} v_{\mathbf{k}_F}^0. \quad (3.2)$$

To cast the high-frequency limit of Eq. (3.1) into a form of the ‘‘extended Drude formula’’,¹ we expand in $\text{Im}\Sigma^R$, evaluate the frequency integral, and bring the result of integration back into the denominator, which yields

$$\sigma_1^{\text{HF}}(\Omega, T) = i \frac{\omega_{p0}^2}{4\pi} \frac{1}{\Omega(1 + \lambda) + i \frac{2C}{3} (\Omega^2 + 4\pi^2 T^2)} \quad (3.3)$$

or

$$\text{Re}\rho_1^{\text{HF}}(\Omega, T) = \frac{4\pi}{\omega_{p0}^2} \frac{2C}{3} (\Omega^2 + 4\pi^2 T^2), \quad (3.4)$$

where HF stands for ‘‘high frequency’’. We remind that Eqs. (3.3) and (3.4) are still valid only the high-frequency limit, defined by Eq. (2.11).

B. Low-frequency regime

We now analyze $\sigma_1(\Omega, T)$ at $\Omega \rightarrow 0$ and finite T , when condition (2.11) is no longer valid.

In what follows, we will need the numerical values of integrals

$$I_n = \int_0^{\infty} \frac{dx}{\cosh^2 x} \frac{1}{(x^2 + \pi^2/4)^{n+1}}, \quad (3.5)$$

in particular, $I_0 = 0.333\dots$, $I_1 = 0.117\dots$, $I_2 = 0.043\dots$. Substituting $\Omega = 0$ into Eq. (3.1) and integrating over ω , we obtain the *dc* resistivity as

$$\rho_1^{\text{LF}}(0, T) = \frac{4\pi}{\omega_{p0}^2} (a_0 C) 4\pi^2 T^2, \quad (3.6)$$

where LF stands for ‘‘low frequency’’ and

$$a_0 = \frac{2}{I_0 \pi^2} = 0.608\dots \quad (3.7)$$

On the other hand, extrapolation of the high-frequency conductivity in Eq. (3.3) to $\Omega = 0$ gives

$$\rho_1^{\text{HF}}(\Omega \rightarrow 0, T) = \frac{4\pi}{\omega_{p0}^2} \frac{2C}{3} 4\pi^2 T^2 \quad (3.8)$$

We see that, in the zero-bubble approximation, the prefactors in Eqs. (3.4) and (3.8) turn out to be very close to each other: $(2/3)/0.608 = 1.097$.

We can also obtain the frequency dependence of $\sigma_1(\Omega, T)$ at $\Omega \rightarrow 0$ by expanding Eq. (3.1) further in Ω and casting the result into the form of Eq. (3.3). Expanding in Ω and evaluating the integrals over ω , we obtain

$$\sigma_1^{\text{LF}}(\Omega, T) = i \frac{\omega_{p0}^2}{4\pi} \frac{1}{a_1 \Omega(1 + \lambda) + ia_0 C \left(4\pi^2 T^2 + a_2 \Omega^2 + ia_3 \frac{(1+\lambda)^2 \Omega^2}{C^2 T^2} \right)}, \quad (3.9)$$

or

$$\rho_1^{\text{LF}}(\Omega, T) = \frac{4\pi}{\omega_{p0}^2} a_0 C \left(4\pi^2 T^2 + a_2 \Omega^2 + a_3 \frac{(1 + \lambda)^2 \Omega^2}{C^2 T^2} \right). \quad (3.10)$$

In Eqs. (3.9) and (3.10), a_0 is the same as in Eq. (3.7) while

$$a_1 = a_0^2 I_1 \pi^4 / 4 = 1.053\dots$$

$$a_2 = \frac{a_0 \pi^4}{4} \int_0^{\infty} \frac{dx}{\cosh^2 x} \frac{1}{(x^2 + \frac{\pi^2}{4})^3} \left[\left(x^2 + \frac{\pi^2}{4} \right) \left\{ 1 - 2x \tanh x + \frac{2}{3} \frac{1 - 2 \sinh^2(x)}{\cosh^2 x} \right\} \left(x^2 + \frac{\pi^2}{4} \right) - 2x^2 \right] = 1.030\dots$$

$$a_3 = \frac{\pi^4 a_0}{32} \left(I_2 - \frac{\pi^2 a_0}{2} I_1^2 \right) = 0.0036\dots \quad (3.11)$$

In the FL regime, the imaginary part of the self-energy,

$\sim CT^2$, must be much smaller than T . Therefore, an ex-

pansion in Ω should be in powers of Ω/CT^2 . This is how the first and the last terms (with coefficients a_1 and a_3 , correspondingly) in the denominator of Eq. (3.9) were obtained. However, because a_3 happens to be numerically very small, we also included the leading term from the expansion in Ω/T (with coefficient a_2). In practice, the last term in Eq. (3.9) can be ignored so that

$$\text{Re}\rho_1^{\text{LF}}(\Omega, T) \approx \frac{4\pi}{\omega_{p0}^2} a_0 C (4\pi^2 T^2 + a_2 \Omega^2), \quad (3.12)$$

which is again very close to the high-frequency form, Eq. (3.4).

Nevertheless, a change in the ratio of the prefactors in the Ω^2 and T^2 terms between the low- and high-frequency regimes indicates that the actual dependence of $\text{Re}\rho_1(\Omega, T)$ is actually more complex than just a sum of the Ω^2 and T^2 terms. We computed $\sigma_1(\Omega, T)$ numerically and found that the Ω and T dependences of $\text{Re}\rho_1(\Omega, T)$ in the entire range $\Omega, T \ll E_F$ are well described by an approximate relation

$$\text{Re}\rho_1(\Omega, T) = \frac{4\pi}{\omega_{p0}^2} \frac{2C}{3} (\Omega^2 + 3.65\pi^2 T^2). \quad (3.13)$$

We see that the ratio of the $\pi^2 T^2$ and Ω^2 terms in $\text{Re}\rho_1(\Omega, T)$ is not equal to 4, but numerically is quite close to 4. Notice, however, that a remarkable agreement between the low- and high frequency limits is valid only within the zero-bubble approximation. We discuss effects not captured by this approximation in Sec. IV.

C. Incoherent regime

Equation (3.4) is valid in the high-frequency regime, as specified by Eq. (2.11). Such a regime always exist in a coherent FL, where $\text{Im}\Sigma_{\mathbf{k}F}^R(\Omega, T) \ll \max\{\Omega, T\}$. However, the optical conductivity of strongly correlated metals is often measured in the incoherent regime where all energy scales are comparable, i.e., $\Omega \sim T \sim \text{Re}\Sigma^R \sim \text{Im}\Sigma^R$. Having this in mind, it is instructive to study the behavior of $\text{Re}\rho_1(\Omega, T)$ in the incoherent regime. In general, calculations in this regime require a detailed knowledge of the electron-electron interaction at all energy scales. We use here a simple model in which $\text{Im}\Sigma^R(\omega, T)$ is assumed to follow the FL form $C(\omega^2 + \pi^2 T^2)$ all the way up to some cutoff frequency Λ and to vanish at larger frequencies. The KK transformation then yields

$$\begin{aligned} \text{Re}\Sigma^R(\omega, T) &= \frac{2C\Lambda\omega}{\pi} - \frac{C}{\pi} (\omega^2 + \pi^2 T^2) \ln \frac{\Lambda + \omega}{|\Lambda - \omega|} \\ &\approx \frac{\lambda\omega}{1 + \frac{\omega^2 + \pi^2 T^2}{\Lambda^2}}. \end{aligned} \quad (3.14)$$

where $\lambda = 2C\Lambda/\pi$. At the last step, we replaced the actual $\text{Re}\Sigma^R(\omega, T)$ by an interpolation formula which describes the limits of both small and large (compared to Λ) frequencies but does not have a kink at $\omega = \Lambda$. These

forms of $\text{Re}\Sigma^R$ and $\text{Im}\Sigma^R$ are substituted into the Kubo formula for the conductivity, Eq. (3.1), and the integral over ω is calculated numerically.

We found that in a wide range of Ω and T , including $\Omega \sim T \sim \Lambda$, the optical resistivity can be well approximated by

$$\text{Re}\rho_1(\Omega, T) \approx \frac{4\pi}{\omega_{p0}^2} 0.64B (\Omega^2 + 3.86\pi^2 T^2). \quad (3.15)$$

We see the same trend as we found earlier in the low-frequency regime: the Ω and T dependencies of the optical resistivity are well approximated by the Ω^2 and T^2 forms, although the actual function is more complex than just the sum of these two terms, and the ratio of the $\pi^2 T^2$ and Ω^2 terms is smaller than 4 but not far from 4.

IV. UMKLAPP PROCESSES

In Sec. II, we showed that any diagram for the conductivity produces the same Ω/T scaling form as indicated in Eq. (1.2), with a prefactor which depends on the electron spectrum. Since no restrictions were imposed on the change in the electron quasimomentum due to the interaction, both the normal and Umklapp processes were implicitly taken into account. The interplay between these two types of processes is different, however, in different frequency regimes.

In the high-frequency regime, as specified by Eq. (2.11), the resistivity is finite already in the presence of only normal processes, provided that Galilean invariance is broken by a lattice. Even on a lattice, however, the leading, $\Omega^2 + 4\pi^2 T^2$ term vanishes in several special cases, e.g., for a quadratic *or* isotropic FS in any D, and for a convex *and* simply-connected in 2D.^{17,18,23} In these cases, the optical resistivity scales as $\max\{\Omega^4, T^4\}$. [The case of an isotropic *and* quadratic spectrum corresponds to a Galilean-invariant FL, the conductivity of which retains a free-electron Drude form regardless of the electron-electron interaction.] In what follows, we assume that the FS does *not* belong to any of the types specified above, so that normal processes do contribute to the leading term in the resistivity. If Umklapp processes are also allowed, they affect the resistivity as well. The prefactor A' in Eq. (1.2) is proportional to the interaction vertex, Γ . In the high-frequency regime, Γ is just a sum of the vertices for normal and Umklapp processes (Γ_N and Γ_U , correspondingly), i.e.,

$$A' \propto \Gamma' = \Gamma_N + \Gamma_U. \quad (4.1)$$

In the opposite limit of $\Omega = 0$, the resistivity of an impurity-free system is non-zero only in the presence of Umklapp scattering. However, once Umklapp processes are allowed, normal processes contribute as well,¹⁹ at least as a correction to the Umklapp contribution (again, if the FS is not of one of the types specified in the preceding paragraph). The effective vertex Γ , entering

Eq. (1.4), is now a non-trivial function of Γ_N and Γ_U which can be represented in the following scaling form

$$A \propto \Gamma = \Gamma_U \Phi(\Gamma_N/\Gamma_U). \quad (4.2)$$

On general grounds, one can infer that $\Phi(x \rightarrow 0) = C_1 + \mathcal{O}(x)$ and $\Phi(x \rightarrow \infty) = C_2$, where $C_{1,2}$ are constants. The ratio Γ_N/Γ_U and the function $\Phi(x)$ itself depend on the details of both the bandstructure and the interaction and are by no means universal. Therefore, prefactors A' and A differ by a non-universal factor, which is expected to be of order one but not specifically close to 1.

Even if, for some reason, normal processes are absent, A and A' still differ because, when calculating the optical resistivity in the high-frequency regime, one expands the Green's functions in the self-energy and averages the result with the difference of the Fermi functions, while in the low-frequency regime the self-energy must be kept in the denominators of the Green's functions. Although it turns out that A and A' almost coincide in the zero-bubble approximation (cf. Sec. III A), there is no guarantee that this remains true if vertex corrections are taken into account.

We conclude this section with a remark in regard to a statement by Rosch and Howell,¹⁷ who argued that the coefficients α_0 and β_0 in $\text{Re}\rho(\Omega, T) = \alpha_0\Omega^2 + \beta_0T^2$ are not, in general, related. For reasons explained above, this statement is correct if $\text{Re}\rho(\Omega, T)$ is supposed to describe the whole range of frequencies: from low to high. However, as we have already emphasized, the formula $\alpha_0\Omega^2 + \beta_0T^2$ with constant α_0 and β_0 does not describe a crossover between the high- and low-frequency regimes. Nevertheless, α and β are universally related in the *high-frequency regime*, where $\beta_0/\alpha_0 = 4\pi^2$.

This section concludes our analysis of the conductivity of a FL. To summarize, we have shown that the scaling form of the optical resistivity in Eq. (1.2) is quite robust. In the high-frequency regime, this form is produced by all diagrams for the conductivity. If vertex corrections are neglected, then one can go beyond the high-frequency regime. It turns out that, with only small changes in the numerical coefficients, Eq. (1.2) form works well beyond its nominal region of validity, i.e., both near the *dc* limit and at such high Ω and T that the FL picture itself is not applicable. In other words, if the Ω and T dependencies of the resistivity are determined by the electron-electron interaction, it is impossible to avoid the FL scaling form with a coefficient of the T^2 term either equal or very close to $4\pi^2$. As discussed in the next Section, this is *not* what the experiment shows.

V. COMPARISON TO EXPERIMENT

A. Summary of experimental observations: Disagreement with the Fermi-liquid theory

Now we turn to the discussion of the existing experimental data on the Ω/T scaling of the optical resis-

tivity. Although the Ω^2 dependence of $\text{Re}\rho(\Omega, T)$ was convincingly demonstrated in “weakly correlated metals” (Au, Ag, and Cu),²⁵ the T dependence, if measured, was found to result from the electron-phonon rather than the electron-electron interaction. This is not surprising since the electron-electron interaction in these metals is relatively weak and one needs to go to very low temperatures to observe the T^2 dependence. To the best of our knowledge, the $\Omega^2 + 4\pi^2T^2$ scaling still has not been verified in weakly correlated metals.

On the other hand, the Ω/T scaling of the optical conductivity in strongly correlated metals has been studied quite extensively; a detailed summary of experimental observations can be found in Ref. 8. The conclusion of these studies is quite surprising: fitting the measured “optical scattering rate” into a phenomenological form

$$\frac{1}{\tau(\Omega, T)} \equiv \frac{4\pi}{\omega_p^2} \text{Re}\rho(\Omega, T) = \text{const} \times (\Omega^2 + b\pi^2T^2) \quad (5.1)$$

has *not* produced b close to 4 in *any* of the cases studied so far. In some cases, e.g., in the heavy-fermion compound URu₂Si₂⁸ above the 17.5 K transition into the “hidden-order” (HO) state and in rare-earth based doped Mott insulators (Ce_{0.095}Ca_{0.05}TiO_{3.04}⁹ and Nd_{0.905}TiO₃¹⁰), b has been found to be close to 1 rather than to 4. On the other hand, a recent study¹¹ of the underdoped cuprate HgBa₂CuO_{4+ δ} reports $b \approx 2.3$, while another study of an organic material from the BEDT-TTF family reports $b \approx 5.6$.¹²

In the preceding sections, we showed that $b \approx 4$ is a robust property of FLs with electron-electron interaction. We must then conclude that even though $1/\tau(\Omega, T)$ in the compounds mentioned above exhibits FL-like dependences on Ω and T , the lack of a FL-like Ω/T scaling indicates that these dependencies do not come only from the electron-electron interaction. In the remainder of this Section, we attempt to explain the discrepancy between the FL theory and the experiment.

B. Elastic vs inelastic contributions to the single-particle self-energy

In this Section, we try to identify a mechanism responsible for deviation of the observed coefficient b from the FL value of 4. In the preceding Sections, we analyzed the conductivity of a FL under an implicit *assumption* that the only scattering mechanism is the electron-electron interaction among itinerant electrons. However, the FL of itinerant electrons is not the only example of a FL. Another example is a FL state formed around magnetic impurities at energies below the Kondo temperature. In the Kondo case, there are two channels of interaction: an elastic one, which contributes an ω^2 term to the imaginary part of the self-energy, and an inelastic or electron-electron one, which contributes an $\omega^2 + \pi^2T^2$ term. The relative weight of these two contributions depends on the strength of the on-site electron-electron interaction,

which can be conveniently parameterized by the Wilson ratio, R .²⁰ In the unitary limit, when $R = 2$, the elastic channel is twice more efficient than the inelastic one, i.e.,

$$\begin{aligned} \text{Im}\Sigma^R(\omega, T) &= B - \frac{2}{3}C' \left(\omega^2 + \frac{1}{2}[\omega^2 + \pi^2 T^2] \right) \\ &= B - C' \left(\omega^2 + \frac{1}{3}\pi^2 T^2 \right), \end{aligned} \quad (5.2)$$

where B is the ω -independent part of the elastic contribution and $C' > 0$. The reduction of the T^2 contribution to $\text{Im}\Sigma_R$ is reflected in the optical scattering rate, which is obtained, as before, by substituting Eq. (5.2) into the Kubo formula (3.1) (in the zero-bubble approximation) and integrating over ω :

$$\frac{1}{\tau(\Omega, T)} = B - \frac{2C'}{3} (\Omega^2 + 2\pi^2 T^2) \quad (5.3)$$

Thus the Kondo FL belongs to a different universality class with $b = 2$. This does not explain the experiment yet because of the *non-metallic* signs of the Ω and T dependences of $1/\tau(\Omega, T)$ in Eq. (5.3), as opposed to the *metallic* signs observed in the experiment at least at the lowest frequencies. However, this gives us an idea to ask: how does a reduction of the inelastic contribution to the self-energy affect the relative weight of the Ω^2 and T^2 terms in the optical conductivity?

To answer this question, we introduce a phenomenological form of the self-energy

$$\text{Im}\Sigma^R(\omega, T) = \Sigma_{\text{el}}(\omega) + C (\omega^2 + \pi^2 T^2). \quad (5.4)$$

The first term describes a contribution of the elastic channel which arises from the energy dependence of the effective scattering cross-section. However, since scattering is elastic, its cross-section does not depend on the temperature (provided that the number and other properties of the scattering centers do not vary with T) and $\Sigma_{\text{el}}(\omega)$ is T -independent. The second term describes the contribution of inelastic electron-electron interaction, which is the same as in a conventional FL. A particular form of $\Sigma_{\text{el}}(\omega)$ is important for determining the actual behavior of the optical conductivity, especially if $\Sigma_{\text{el}}(\omega)$ is a sharp function of ω , as it is the case for resonant scattering, considered in the next Section. For the time being, however, we assume only that $\Sigma_{\text{el}}(\omega)$ is an analytic function of ω and expand it to second order in ω as

$$\Sigma_{\text{el}}(\omega) = \Sigma_{\text{el}}(0) + \Sigma'_{\text{el}}(0)\omega + aC\omega^2, \quad (5.5)$$

where the constant C [the same as in Eq. (5.4)] was factored out for convenience, and a is another constant which can be of either sign. We call the elastic contribution “metallic” if $a > 0$ and “non-metallic” if $a < 0$. On the other hand, the inelastic contribution is always metallic because $C > 0$ (which is not the case for the Kondo model). Combining Eqs. (5.4) and (5.5), we obtain

$$\text{Im}\Sigma^R(\omega, T) = \Sigma_{\text{el}}(0) + \Sigma'_{\text{el}}(0)\omega + C [a\omega^2 + (\omega^2 + \pi^2 T^2)]. \quad (5.6)$$

The $a\omega^2$ term mimics the ω^2 dependence of the inelastic contribution but does not have its T^2 counterpart. We emphasize that the ω and T dependencies of the inelastic contribution should be consistent with the fermionic first-Matsubara-frequency rule, which stipulates that the inelastic term in Eq. (5.4) must vanish upon replacing ω by $\pm i\pi T$. This rule, which is obviously satisfied with our choice for the inelastic part, does not allow for changes in the relative weight of the ω^2 and T^2 terms in this part. Next, we substitute Eq. (5.4) into Eq. (3.1), integrate over ω , upon which the linear-in- ω term in $\text{Im}\Sigma^R(\omega, T)$ vanishes, and obtain the optical scattering rate as

$$\frac{1}{\tau(\Omega, T)} = \frac{1}{\tau_0} + \frac{2}{3}(a+1)C [\Omega^2 + b\pi^2 T^2] \quad (5.7)$$

with

$$b = \frac{a+4}{a+1}. \quad (5.8)$$

The residual term, $1/\tau_0$, contains a contribution from static disorder (not considered explicitly here), and we absorbed Σ_{el} into this term as well.

Now we discuss constraints imposed on the parameter a , and thus on b . For $a < -1$, the prefactor of the second term in Eq. (5.7) is negative, i.e., the Ω and T dependencies of $1/\tau(\Omega, T)$ are non-metallic. Since this does not correspond to any of the experiments, we discard this possibility. The special case of $a = -1$ corresponds to $1/\tau(\Omega, T)$ which depends only on T but not on Ω . Discarding this possibility as well, we focus on the range $-1 < a < \infty$, which corresponds to $1 \leq b < \infty$. The FL value of $b = 4$ is reproduced for $a = 0$. The opposite limit of $a = \infty$ (and thus $b = 1$) corresponds to a purely elastic scattering mechanism. The range $1 < b < 4$ corresponds to a mixture of elastic and inelastic mechanisms with $a > 0$, i.e., with a metallic sign of the elastic contribution, whereas $b > 4$ corresponds to a non-metallic elastic contribution with $-1 < a < 0$, although the Ω and T dependences of $1/\tau(\Omega, T)$ in this case are still metallic.

According to this classification scheme, the value of $b \approx 1$, reported in Refs. 8–10 for the U, Ce, and Nd-based compounds, indicates a purely elastic scattering mechanism ($a = \infty$). The value of $b \approx 2.3$ (and thus $a \approx 1.3$), reported in Ref. 11 for the Hg-based underdoped cuprate, points at a mixture of elastic and inelastic mechanisms with comparable weights, and with a metallic sign of the elastic contribution. Finally, $b \approx 5.6$ (and thus $a \approx -0.35$), reported in Ref. 12 for the organic material, also corresponds to a mixture of the two mechanisms but with a non-metallic sign of the elastic contribution.

The deviation from the FL behavior is the most dramatic for the $b = 1$ case, where it appears that the electron-electron interaction does not play any role. However, this conclusion would be incorrect. In the next Section, we discuss one example of a purely elastic scattering mechanism, i.e., scattering from resonant levels, and apply this model to the URu₂Si₂ data. We will see that, while the optical conductivity can be explained by

resonant-level scattering alone, an explanation of the T dependence of the dc resistivity requires invoking a sufficiently strong electron-electron interaction.

C. Scattering from resonant levels: the case of URu₂Si₂

In this section, we discuss the model of purely elastic scattering from resonant levels, located at energy ω_0 away from the Fermi energy and of width γ . The self-energy in this case is given by

$$\text{Im}\Sigma^R(\omega, T) = \Sigma_{\text{el}}(\omega) = \frac{C_0\gamma}{(\omega - \omega_0)^2 + \gamma^2}. \quad (5.9)$$

At $T = 0$, the corresponding optical scattering rate is given by

$$\frac{1}{\tau(\Omega, 0)} = \frac{C_0}{\Omega} \left[\arctan \frac{\Omega - \omega_0}{\gamma} + \arctan \frac{\Omega + \omega_0}{\gamma} \right]. \quad (5.10)$$

If the resonant level coincides with the Fermi energy, $1/\tau(\Omega, 0)$ is purely non-metallic, i.e., it decreases as Ω increases. If the resonant level is away from the Fermi energy, $1/\tau(\Omega, 0)$ is a non-monotonic function of Ω with a maximum at $\Omega \sim \omega_0$ (see Fig. 4). The origin of the maximum is clear: as Ω increases from zero to ω_0 , the rate of transitions from the Fermi energy to the resonant levels increases. When Ω becomes larger than ω_0 , the rate decreases because now the energy interval from the Fermi energy to the resonant level constitutes only a fraction of the photon energy. Expanding Eq. (5.9) near $\omega = 0$ as

$$\text{Im}\Sigma^R(\omega) = C_0\gamma \left[\frac{1}{\omega_0^2 + \gamma^2} + \frac{2\omega\omega_0}{(\omega_0^2 + \gamma^2)^2} + \frac{3\omega_0^2 - \gamma^2}{(\omega_0^2 + \gamma^2)^3} \omega^2 \right] \quad (5.11)$$

and substituting (5.11) into (3.1), we obtain

$$\frac{1}{\tau(\Omega, T)} = \text{const} + \frac{C_0\gamma(3\omega_0^2 - \gamma^2)}{(\omega_0^2 + \gamma^2)^3} (\Omega^2 + \pi^2 T^2). \quad (5.12)$$

(The linear in ω term in Eq. (5.11) vanishes by parity.) Already for a moderately narrow level, i.e., for $\gamma < \omega_0\sqrt{3}$, the signs of both the Ω and T dependences of $1/\tau(\Omega, T)$ are metallic, and $b = 1$. The behavior of $1/\tau(\Omega, T)$ over a larger range of Ω and T is obtained by substituting Eq. (5.9) into the Kubo formula (3.1) and computing the integral over ω numerically. The results are shown in Fig. 5. To compare to the experimental data on URu₂Si₂ from Ref. 8, shown in Fig. 7, we choose $\omega_0 = 12.5$ meV to match the position of the peak in the data. All other energies are measured relative to ω_0 . In Fig. 5, $\gamma = 0.2\omega_0$, and the temperatures are chosen to coincide with the absolute temperatures used in the experiment (18, 22, and 25 K). Comparing Figs. 5 and 7, we see that the model reproduces the characteristic features of the data, i.e., a non-monotonic dependence of $1/\tau(\Omega, T)$ on Ω , as well

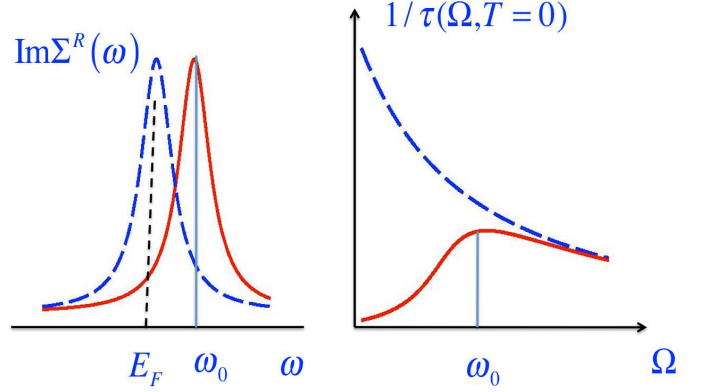


FIG. 4. (color on-line). Imaginary part of the fermionic self-energy, Eq. (5.9), (left) and optical scattering rate at $T = 0$, Eq. (5.12) (right) for scattering at resonant impurities.

as an (approximate) isobestic point at $\Omega \approx \omega_0$, where $1/\tau(\Omega, T)$ apparently does not depend on T . The very existence of the isobestic point implies that the data cannot be described by Eq. (1.2) with a T -independent prefactor A' . Nevertheless, we follow the same protocol as used in Ref. 8, i.e., we fit the Ω dependence of the computed $1/\tau(\Omega, T)$ into an Ω^2 function (shown by dashed lines in Fig. 5), then fit the intercept $1/\tau(\Omega \rightarrow 0, T)$ into a T^2 function (shown in Fig. 6), and take the ratio of the slopes of the T^2 and Ω^2 fits. This procedure gives $b \approx 0.9$, which is within the margin of error of the experimental value $b = 1 \pm 0.1$.⁸

The behavior of $1/\tau(\Omega, T)$ in the Ce and Nd compounds (Refs. 9 and 10, correspondingly) is qualitatively similar to that in URu₂Si₂, although the ranges of Ω and T are drastically different. In Nd_{0.905}TiO₃, $1/\tau(\Omega, T)$ scales as Ω^2 up to about 0.1 eV, followed by a maximum at ≈ 0.27 eV. The $\Omega = 0$ intercept of $1/\tau$ scales as T^2 over a wide temperature range: from 29 to 295 K.²⁸ In Ce_{0.095}Ca_{0.05}TiO_{3.04}, $1/\tau(\Omega, T)$ scales as Ω^2 also up to about 0.1 eV, followed by a tendency to saturation; but the maximum is not yet revealed at the highest frequency measured (≈ 0.14 eV). The $\Omega = 0$ intercept also scales as T^2 over a wide range of temperatures. These similarities suggest that, despite obvious differences in composition and energy scales in U, Ce, and Nd compounds, the optical response in all three cases is governed by the same mechanism.

Elucidation of the microscopic mechanism of resonant levels is beyond the scope of this work, and we make just a brief comment in this regard. It is very unlikely that clean samples studied in Refs. 8–10 contained considerable amounts of *extrinsic* resonant impurities. Therefore, resonant states must be *intrinsic* to these compounds. We surmise that f -electrons of U, Ce, and Nd atoms, although arranged into a sublattice, play the role of *incoherent* resonant levels at sufficiently high energy scales probed in optical measurements.

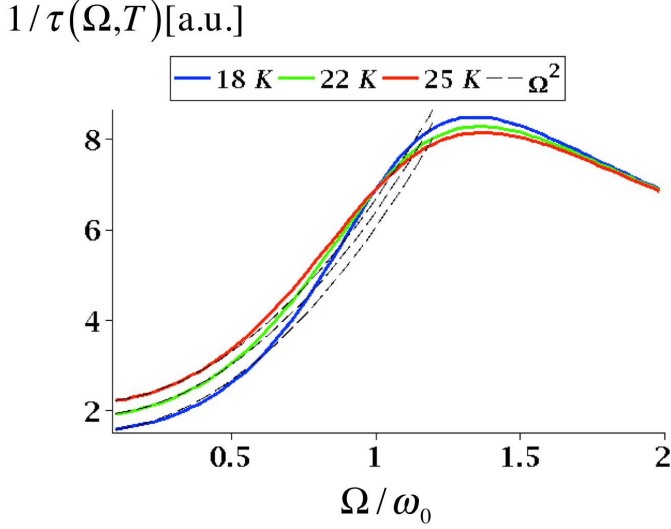


FIG. 5. (color on-line). Optical self-energy in the resonant-impurity model as a function of frequency at several temperatures. Absolute values of temperatures are fixed by choosing $\omega_0 = 12.5$ meV and $\gamma = 0.2\omega_0$. Dashed lines show Ω^2 fits of the actual dependencies.

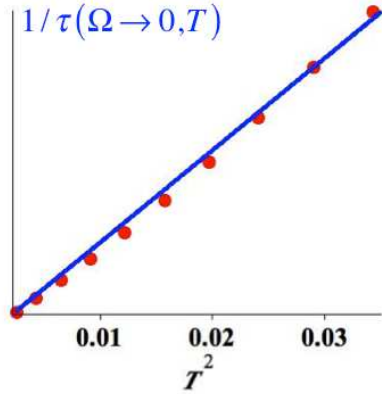


FIG. 6. (color on-line). The intercept, $1/\tau(\Omega \rightarrow 0, T)$, in the resonant impurity model as a function of $(T/\omega_0)^2$.

D. Combined effect of the electron-electron and resonant-level scattering mechanisms

Although the resonant-scattering model explains the results of optical measurements, this model alone cannot explain the temperature dependence of the dc resistivity. Above the superconducting transition temperature (≈ 1 K) in URu_2Si_2 , both the a - and c -axis resistivities increase with T in a quadratic manner within the HO phase, exhibit a kink at HO T_c^{HO} , and continue to increase up to about 75 K, where ρ_a goes through a broad maximum whereas ρ_c starts to saturate.^{29,31,32} The slopes of the increasing parts in $\rho_{a,c}$, both below and above T_c^{HO} , are largely independent of the residual resistivity,³⁰ which indicates that the T -dependence

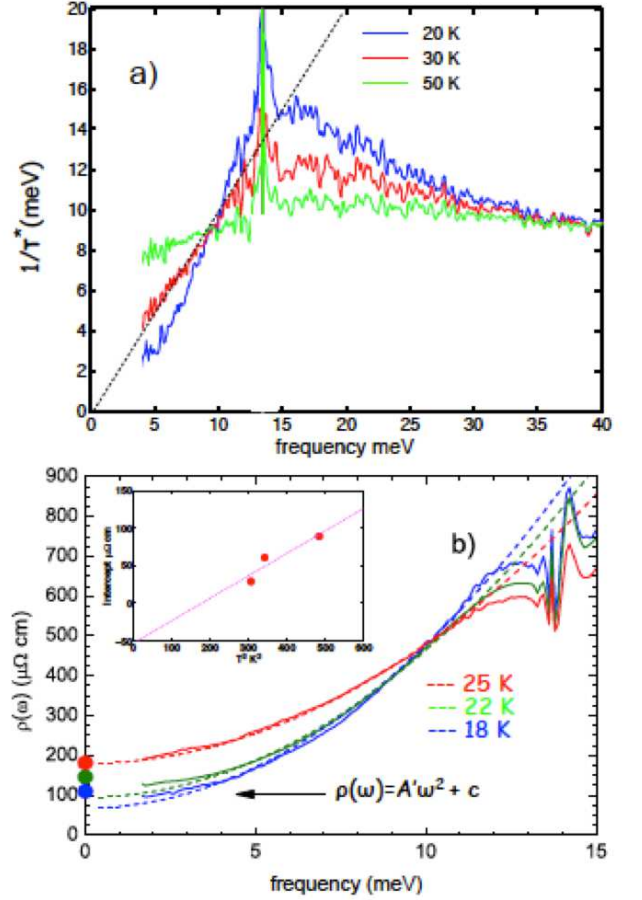


FIG. 7. (color on-line). Experimental results for in URu_2Si_2 from Ref. 8. a) Optical scattering rate $1/\tau(\Omega, T)$. b) The optical resistivity at lower frequencies from the refined reflectivity.

comes from an intrinsic mechanism. On the contrary, the T dependence of the dc resistivity in the resonant-scattering model is purely *non-metallic*. Indeed, it is easy to see that the dc conductivity,

$$\sigma(0, T) = \frac{\omega_{p0}^2}{8\pi} \int d\omega \left(-\frac{\partial n_F}{\partial \omega} \right) \frac{1}{\text{Im}\Sigma^R(\omega)} \quad (5.13)$$

with $\text{Im}\Sigma^R(\omega)$ from Eq. (5.9), increases with T as T^2 ; therefore, $\rho(0, T) = 1/\sigma(0, T)$ decreases with T . In order to reproduce the metallic sign of $\rho(0, T)$, at least for T below 75 K, one needs to bring in the inelastic electron-electron interaction with $\text{Im}\Sigma^R(\omega, T)$ given by Eq. (1.1). This seems to defy the purpose of the preceding analysis, as we have argued that the optical data cannot be explained by an inelastic mechanism. It turns out however, that a combination of elastic and inelastic mechanisms explains both the dc and optical data. In the “combined”

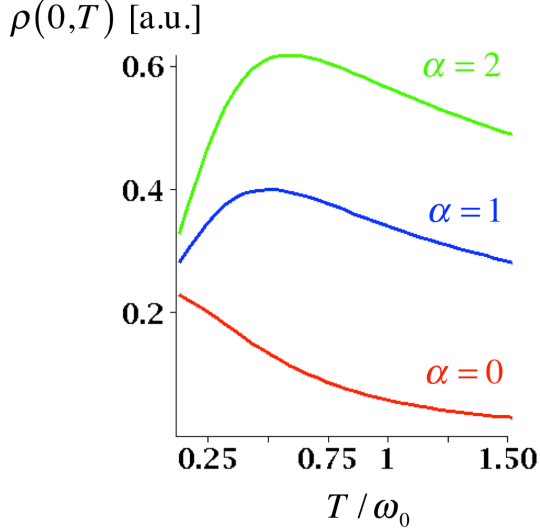


FIG. 8. (color on-line). *dc* resistivity (arbitrary units) for a model form of the self-energy which combines resonant-level and electron-electron contributions, Eq. (5.14). Temperature is measured in units of the resonant-level energy, ω_0 , which is also chosen to coincide with the cutoff energy Λ . The resonant-level width $\gamma = 0.2\omega_0$. Parameter α , defined by Eq. (5.15), measures the relative strength of the two contributions.

model, the total self-energy is a sum of two contributions

$$\text{Im}\Sigma^R(\omega, T) = \frac{C_0\gamma}{(\omega - \omega_0)^2 + \gamma^2} + C(\omega^2 + \pi^2 T^2) F\left(\frac{\sqrt{\omega^2 + \pi^2 T^2}}{\Lambda}\right). \quad (5.14)$$

This equation is the same as we introduced in Eq. (5.4), except for now the electron-electron contribution contains a smooth cutoff function $F(x)$, defined in such a way that $F(0) = 1$ and $F(x)$ falls off faster than $1/x^2$ for $x \gg 1$. The function $F(x)$ is chosen to reproduce a slow decrease of the measured *a*-axis resistivity at higher temperatures. (Since optical experiments probe the basal-plane conductivity, we focus on this case.) To minimize the number of free parameters, we set $\Lambda = \omega_0$. The relative strength of two contributions to $\text{Im}\Sigma^R(\omega, T)$ in Eq. (5.14) is controlled by a dimensionless parameter

$$\alpha \equiv \frac{C\omega_0^4}{C_0\gamma}. \quad (5.15)$$

Larger values of α correspond to a larger electron-electron and smaller resonant-level contribution, and vice versa. Using the small- ω expansion in Eq. (5.11), it is easy to show that $d\rho(0, T)/dT|_{T \rightarrow 0}$ is positive, i.e., “metallic”, already for $\alpha > 1/4$. The dependence of $\rho(0, T)$ over the entire temperature range is obtained by numerical integration of Eq. (5.13) with $\text{Im}\Sigma^R$ from Eq. (5.14). The resulting profiles of $\rho(0, T)$ are shown in Fig. 8 for $\alpha = 0, 1, 2$. As we see, the electron-electron

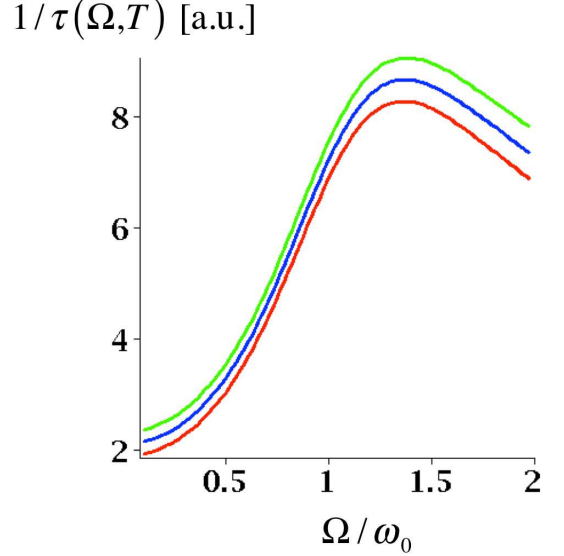


FIG. 9. (color on-line). Optical scattering rate (arbitrary units) for a model form of the self-energy which combines resonant-level and electron-electron contributions, Eq. (5.14). Frequency is measured in units of ω_0 . $T = 22$ K, $\gamma = 0.2\omega_0$. From top to bottom: $\alpha = 0$ (red), $\alpha = 1$ (blue), $\alpha = 2$ (green).

contribution leads to a qualitative change in $\rho(0, T)$: a purely non-metallic T dependence with resonant levels alone ($\alpha = 0$) is transformed into a curve with a maximum ($\alpha = 1, 2$). The $\alpha = 2$ curve is already similar to the measured profile of $\rho(0, T)$, which increases almost three-fold when T is varied in between T_c^{HO} (chosen as the lowest temperature in Fig. 8) and the temperature corresponding to a maximum resistivity.^{29,31,32} On the contrary, the optical resistivity is largely unaffected by the electron-electron contribution. Figure 9 shows the frequency dependence of the optical scattering rate at fixed temperature ($= 22$ K) for the same values of α ($= 0, 1, 2$) as in the *dc* case (Fig. 8). As it is obvious from the figure, $1/\tau(\Omega, T)$ is practically the same for all three values of α , except for a small overall shift. Repeating the same procedure as was applied to the numerical data in Figs. 5 and 6, we again arrive at the result that coefficient b in Eq. (5.1) is very close to 1.

The results presented above indicate that the electron-electron and resonant-level contributions to the self-energy affect different parts of the frequency range: whereas the electron-electron contribution is largely responsible for the T dependence of the *dc* resistivity and has practically no effect on the high-frequency optical resistivity, the resonant-level contribution determines the optical resistivity but plays only a secondary role in controlling the *dc* resistivity. This happens because *dc* and optical measurements probe different parts of the electron spectrum (cf. Fig. 10). At sufficiently low temperatures, i.e., at $T \ll \omega_0$, a *dc* measurement probes the spectrum in the region $\omega \sim T \ll \omega_0$, where both contributions to the self-energy vary smoothly with ω (as ω^2).

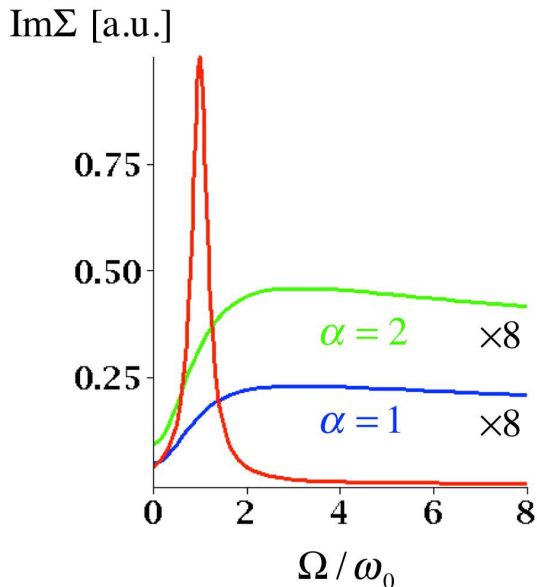


FIG. 10. (color on-line). Resonant-level (a sharply peaked curve) and electron-electron contributions to the imaginary part of the self-energy. The electron-electron parts correspond to $\alpha = 1, 2$ and were multiplied by a factor of 8 for clarity.

The resulting T dependence of $\rho(0, T)$ is just a sum of two T^2 terms with opposite signs, and the electron-electron contribution wins this competition rather easily. On the other hand, the optical scattering rate is controlled by the region $\omega \sim \omega_0$, where the resonant-level contribution has a sharp peak and thus dominates over the electron-electron one, even if the latter is strong enough to control the dc resistivity.

Concluding this section, we would like to emphasize the importance of a sharp feature in the elastic contribution to the self-energy, $\Sigma_{el}(\omega)$. Indeed, the classification scheme of different behaviors of $1/\tau(\Omega, T)$ based on the magnitude and sign of the coefficient a , as defined by Eq. (5.5), would predict substantially different values of b for the values of the parameter α used above. It is easy to see that, in the resonant scattering model, $a = 3/\alpha$ which, according to Eq. (5.8), implies that $b = (4\alpha + 3)/(\alpha + 3)$. This formula gives $b = 1$ for $\alpha = 0$; $b = 7/4 \approx 1.75$ for $\alpha = 1$; and $b = 11/5 \approx 2.2$ for $\alpha = 2$. Nevertheless, fitting $1/\tau(\Omega, T)$ curves computed with a full form of Σ_{ee} rather than with its Taylor expansion, we obtained $b \approx 1$ in all of these cases. The reason for this discrepancy is that the Taylor expansion is not applicable near a sharp peak Σ_{ee} , and one needs to use the classification scheme based on Eqs. (5.7) and (5.8) with certain care.

VI. SUMMARY

The main purpose of this paper was to highlight the universality of the FL result for the optical resistivity,

Eq. (1.2). We showed that, within the Kubo formalism which takes full account of vertex corrections to the conductivity, Eq. (1.2) holds for an arbitrary lattice and for any form of the electron-electron interaction, as long as the system remains a FL and is away from nesting and Van Hove singularities. In fact, the optical resistivity turns out to be more universal than the single-particle self-energy: whereas the latter is described by the conventional form given by Eq. (1.1) only in canonical FLs, i.e., in $D > 2$, and deviates from this form in non-canonical FLs i.e., in $1 < D \leq 2$, the former is given by Eq. (1.2) both for canonical and non-canonical FLs. We showed that a particular scaling form in Eq. (1.2) takes its roots in analytic properties of the optical conductivity along the Matsubara axis and is consistent with the bosonic first-Matsubara-frequency rule.

If a system contains not only of itinerant electrons but also localized degrees of freedom (magnetic moments or resonant levels), the functional form of the optical resistivity changes, as specified by Eq. (5.1). The magnitude of the coefficient b in this equation depends on the interplay between inelastic (electron-electron) and elastic scattering mechanisms. Completely inelastic electron-electron scattering corresponds to $b = 4$; completely elastic scattering from, e.g., resonant levels, gives $b = 1$; intermediate cases, where elastic and inelastic channels are mixed, correspond to $1 < b < \infty$.

As far as the existing experiments are concerned, the value of $b = 4$ has never been reported. In some cases, including the latest detailed study of the optical conductivity in URu_2Si_2 (Ref. 8), the coefficient b has been found to be close to 1, which indicates a completely elastic scattering mechanism; a recent study of the Hg-based underdoped cuprate reports $b \approx 2.3$; yet another study of the BEDT-TTF organic material reports $b \approx 5.6$. We considered a simple model of scattering from resonant levels, and showed it is capable of reproducing the major features of the optical resistivity in URu_2Si_2 above T_c^{HO} . On the other hand, the T dependence of the dc resistivity can only be explained in a model which combines elastic and inelastic electron-electron scattering mechanism. We deliberately refrained from identifying a microscopic nature of resonant levels, except for stating that they are not likely to be extrinsic resonant impurities. More likely, deep f states of rare earth atoms play the role of incoherent resonant scatterers at rather high energy scales probed in optical measurements.

If this picture is correct, it tells us something new about a crossover between coherent and incoherent regimes in heavy-fermion materials. The conventional scenario of this crossover is that the only energy scale is the Kondo temperature (T_K). Above T_K , localized magnetic moments scatter electrons incoherently, as in diluted Kondo alloy. Below T_K , a (heavy) FL state is formed and localized moments do not scatter electrons anymore but participate in formation of a coherent Bloch state. The low-energy FL state is supposed to have all the attributes of a standard FL, in particular, the coef-

ficient b must be equal to 4. This scenario is probably correct as long as the evolution of the system is traced along the temperature axis. Optical measurements add one more dimension: frequency. In the presence of elastic scattering, the variations of temperature and frequency do not have the same physical consequences because the scattering cross-section depends on the electron energy, and thus on the frequency of light, but not on the temperature. It appears that the crossover between the incoherent and coherent regimes along the frequency axis contains an intermediate interval, where localized states scatter itinerant electrons neither as Kondo spins nor as screened Kondo clouds but rather as resonant levels.

Regardless of the validity of a particular model for elastic scattering, we hope that our paper will help to recognize the importance of the interplay between Ω and T dependencies in the optical data. We believe that, on par with much studied recently Wiedemann-Franz law which, if satisfied, indicates not only the FL nature of the ground state but also complete elasticity of the underlying scattering mechanism, systematic studies of the coefficient b can tell us something new about the interplay between elastic and inelastic channels in strongly

correlated electron systems.

ACKNOWLEDGMENTS

We are particularly thankful to T. Timusk for motivating us to perform this study, and to all authors of Ref. 8 for allowing us to use their data in our paper. Helpful discussions with D. Basov, M. Broun, D. Dessau, P. Coleman, S. Dodge, M. Dressel, A. Georges, K. Ingersent, Y.-B. Kim, P. Kumar, M. Kennett, D. van der Marel, A. Millis, U. Nagel, T. Room, M. Sheffler, D. Tanner, A.-M. Tremblay, and V. I. Yudson are gratefully acknowledged. The work was supported by nsf-dmr 0906953 and Humboldt foundation (A. V. Ch.), and by nsf-dmr 0908029. We are thankful to MIPPKS Dresden (A.V. Ch. and D.L.M.), the Aspen Center of Physics (A. V. Ch.), the Ruhr-University Bochum (A.V. Ch.), Simon Fraser University (D.L.M.), and Swiss NSF “QC2 Visitor Program” at the University of Basel (D.L.M.) for hospitality during the various phases of this work. The Aspen Center of Physics is supported in part by the NSF Grant 1066293.

-
- ¹ D. N. Basov, R. D. Averitt, D. van der Marel, M. Dressel, and K. Haule, *Rev. Mod. Phys.* **83**, 471 (2011).
- ² A. V. Chubukov and D. L. Maslov (unpublished).
- ³ L. D. Landau and I. J. Pomeranchuk, *Phys. Z. Sowjetunion* **10**, 649 (1936); *Zh. Eksp. Teor. Fiz.* **7**, 379 (1937).
- ⁴ W. G. Baber, *Proc. Roy. Soc. London* **158**, 383 (1937).
- ⁵ G. M. Eliashberg, *Sov. Phys. JETP* **14**, 886 (1962).
- ⁶ R. N. Gurzhi, *Sov. Phys. JETP* **35**, 673 (1959).
- ⁷ E. M. Lifshitz and L. P. Pitaevskii, *Physical Kinetics*, (Oxford, Pergamon Press, 1981).
- ⁸ U. Nagel, T. Uleksin, T. R  om, R.P.S.M. Lobo, P. Lejay, C.C. Homes, J. Hall, A.W. Kinross, S. Purdy, T.J. Williams, G.M. Luke, T. Timusk, arXiv:1107.5574.
- ⁹ T. Katsufuji and Y. Tokura, *Phys. Rev. B* **60**, 7673 (1999).
- ¹⁰ J. Yang, J. Hwang, T. Timusk, A. S. Sefat, and J. E. Greedan, *Phys. Rev. B* **73**, 195125 (2006).
- ¹¹ S. I. Mirzaei, D. Stricker, J. N. Hancock, C. Berthod, A. Georges, E. van Heumen, M. K. Chan, X. Zhao, Y. Li, M. Greven, N. Bari  ic, D. van der Marel, arXiv:1207.6704.
- ¹² M. Dressel, *J. Phys. Condens. Matter* **23**, 293201 (2011); S. Yasin, M. Dumm, B. Salameh, P. Batail, C. Mezi  re, and M. Dressel, *Eur. Phys. J. B* **79**, 383 (2011).
- ¹³ P. E. Sulewski, M. B. Maple, M. S. Torikachvili, J. L. Smith, and Z. Fisk et al. *Phys. Rev. B* **38**, 5338 (1988).
- ¹⁴ T. Katsufuji, M. Kasai, and Y. Tokura, *Phys. Rev. Lett.* **76**, 126 (1996).
- ¹⁵ D. N. Baslov, E. J. Singley, and S. V. Dordevic, *Phys. Rev. B* **65**, 054516 (2002).
- ¹⁶ A. Georges, G. Kotliar, W. Krauth, and M. Rozenberg, *Rev. Mod. Phys.* **68**, 13 (1996).
- ¹⁷ a) A. Rosch and P. C. Howell, *Phys. Rev. B* **72**, 104510 (2005); b) A. Rosch, *Ann. Phys.* **15**, 526 (2006).
- ¹⁸ D. L. Maslov, V. I. Yudson, and A. V. Chubukov *Phys. Rev. Lett.* **106**, 106403 (2011); H. K. Pal. V. I. Yudson, and D. L. Maslov, *Lith. J. Phys.* **52**, 142 (2012); arXiv:1204.3591.
- ¹⁹ a) H. Maebashi and H. Fukuyama, *J. Phys. Soc. Japan* **66**, 3577 (1997); b) *ibid.* **67**, 242 (1998).
- ²⁰ A. C. Hewson, *The Kondo Problem to Heavy Fermions*, (Cambridge University Press, Cambridge, 1993).
- ²¹ K. Michaeli and A. M. Finkel’stein, *Phys. Rev.* **B80**, 115111 (2009).
- ²² A. M. Tsvelik and A. V. Chubukov, *Phys. Rev. Lett.* **98**, 237001 (2007).
- ²³ R. N. Gurzhi, A. I. Kopeliovich, and S. B. Rutkevich, *JETP Lett.* **56**, 159 (1982); c) *Adv. Phys.* **36**, 221 (1987).
- ²⁴ A. O. Lyakhov and E. G. Mishchenko, *Phys. Rev. B* **67**, 041304 (2003).
- ²⁵ R. T. Beach and R. W. Christy, *Phys. Rev. B* **16**, 5277 (1977); G. R. Parkins, W. E. Lawrence, and R. W. Christy, *Phys. Rev. B* **23**, 6408 (1981).
- ²⁶ A. J. Millis and P. A. Lee, *Phys. Rev. B* **35**, 394 (1987). The correct value of b in this work should be $b = 4$ (A.J. Millis, private communication).
- ²⁷ D. N. Baslov, E. J. Singley, and S. V. Dordevic, *Phys. Rev. B* **65**, 054516 (2002).
- ²⁸ Notice that the slopes of the T^2 dependences of the dc resistivity and $1/\tau(\Omega \rightarrow 0, T)$ are *different*, see Fig. 11 in Ref. 10. As we discussed in Sec. IV, this indicates the difference in the interplay between normal and Umklapp scattering at low and high frequencies.
- ²⁹ T. T. M. Palstra, A. A. Menovsky, and J. A. Mydosh, *Phys. Rev. B* **33**, 6527 (1986).
- ³⁰ T. Timusk, private communication.
- ³¹ A. J. Dirkmaat, T. Endstra, E. A. Knetsch, G. J. Nieuwenhuys, J. A. Mydosh, A. A. Menovsky, F. R. de Boer, and Z. Tarnawski, *Phys. Rev. B* **41**, 2589 (1990).

- ³² Z. Zhu, E. Hassinger, Z.Xu, D. Aoki, J. Flouquet, and K. Behnia, *Phys. Rev. B* **80**, 172501 (2009).